Nitsche's energetic BEM-FEM coupling for wave propagation in 2D multidomains

Alessandra Aimi, Sara Cattivelli, Franz Chouly, Chiara Guardasoni

Nitsche's energetic BEM-FEM coupling for wave propagation in 2D multidomains

Alessandra Aimi[1], Sara Cattivelli[1], Franz Chouly[*2], and Chiara Guardasoni[†1]

[1]Department of Mathematical, Physical and Computer Sciences, University of Parma, 43124 Parma, Italy

[2]Universidad de la República, Facultad de Ciencias, Centro de Matemática, IRL-2030 CNRS IFUMI, 11400 Montevideo, Uruguay

Abstract

This paper introduces a novel method for coupling the Boundary Element Method (BEM) and the Finite Element Method (FEM) to solve the wave equation. The proposed approach is based on two key components: 1) energetic space-time BEM and FEM formulations and 2) Nitsche's method for the weak enforcement of transmission conditions. Stability analysis for the weak coupled problem and its discrete counterpart is performed through energy arguments. Several numerical results are presented and discussed, showing the effectiveness of the proposed technique.

1 Introduction

The coupling of the Boundary Element Method (BEM) and the Finite Element Method (FEM) has garnered significant interest in the numerical solution of Partial Differential Equations (PDEs) and evolution problems. This hybrid approach combines the advantages of BEM, which is well-suited for handling boundary conditions and infinite domains, with the flexibility of FEM for complex geometries and material properties. Pioneering works have been published in the late seventies [12, 13, 26, 40] that have laid a robust foundation for BEM-FEM coupling techniques, highlighting their potential for enhancing numerical simulations (see as well the review [36]).

In this paper, we present a novel method for coupling BEM with FEM to solve the wave equation, as a prototype of second order linear hyperbolic problem: a Nitsche's approach combines weakly both methods in an energy setting. In fact, the energetic BEM formulation provides a robust framework for capturing the dynamics of wave propagation, while Nitsche's technique ensures stable and accurate weak enforcement of transmission conditions at the interface between BEM and FEM subdomains. It allows potentially non-matching discretizations without Lagrange multipliers. This combination leverages the strengths of both approaches to achieve efficient and reliable numerical solutions. It is a first step before tackling more challenging problems involving elasticity, three-dimensional problems and/or contact and friction conditions, see the related and recent works [4, 28], and references therein.

The main contributions of this work are as follows. First, we develop a coupling scheme that integrates energetic BEM with FEM using Nitsche's method. This scheme is designed to handle the wave equation. Second, we conduct a thorough stability analysis, supported by energy estimates, to demonstrate the robustness of our approach. Third, we present new numerical results and compare them with existing methods to validate the effectiveness of our proposed technique.

Let us put our work in perspective. Nitsche's method has been formulated first in [33], see [16, 15, 18, 24, 38, 39] and references therein for more details. It has been extended to interface problem in [9], see also [21] for a comparison between Nitsche's and mortar techniques for small strain elasticity, as well as related

[*] *Corresponding author:* fchouly@cmat.edu.uy.

[†] A. Aimi and C. Guardasoni are members of INdAM-GNCS

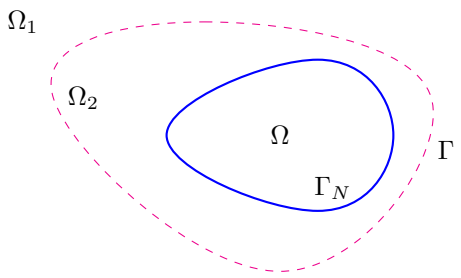

Figure 1: Model problem: the bounded domains Ω, Ω_2 and the unbounded domain Ω_1, as well as the boundary Γ_N of Ω and the interface Γ between Ω_2 and Ω_1.

recent references, such as [17, 23, 25, 27, 32, 35], to mention just a few. The state-of-the-art in BEM-FEM coupling for wave equations includes [3, 6], which explore energetic BEM-FEM coupling in two and three dimensions. In this context, weak imposition of boundary conditions is presented in [5]. Additional relevant studies include [1, 7, 8, 20, 22, 37] and [11, 14, 29]. In the stationary case, the work by Betcke et al. [10] is the first, to the best of our knowledge, to present a Nitsche's BEM-FEM coupling.

This paper is structured as follows. Section 2 describes the setting of BEM-FEM coupling for an interface problem involving Poisson's equation and derives a Nitsche's formulation. The complete discrete approximation is detailed in Section 3. A discrete energy estimate for the approximation technique is provided in Section 4, that ensures the stability of the coupling under appropriate assumptions on the numerical parameters. Numerical results are presented and discussed in Section 5.

2 Setting and analysis

We consider the simple setting of a scalar wave equation in a 2D unbounded domain, with transmission conditions between the interior and exterior of a domain. To make the paper self-contained, we then recall the standard energetic BEM-FEM coupling [3], followed by the introduction of the Nitsche's approach. Some energy considerations will be done throughout the Section.

2.1 Model problem

Let $\Omega \subset \mathbb{R}^2$ be an open set, with Lipschitz boundary Γ_N. Let Ω_1 and Ω_2 be a partition of $\mathbb{R}^2 \setminus \Omega$ into an exterior and an interior domain, respectively. We denote by Γ the interface between the two domains, that we suppose Lipschitz (see Figure 1).

We denote by n_i the outward unit normal to the interface Γ to the domain Ω_i, $i = 1, 2$, so that $\mathrm{n}_1 = -\mathrm{n}_2$. Having fixed a final time instant of analysis $T \in \mathbb{R}^+$, we are interested in finding the solution to the following problem: $u_i : [0, T] \times \Omega \to \mathbb{R}$, $i = 1, 2$ to

$$\rho_i \ddot{u}_i - \mu_i \Delta u_i = \rho_i f_i, \qquad \text{in } (0, T) \times \Omega_i, \tag{1}$$

complemented with the other conditions below. Above we used the notation Δ for the Laplace operator, $\ddot{u}_i := \partial^2 u_i / \partial t^2$ for the second-order derivative in time, and as well we will use the notation $\dot{u}_i := \partial u_i / \partial t$ for the first order derivative. Still above, f_i is the source term, μ_i and ρ_i are the bulk modulus and the material density respectively, defining the wave speed $c_i = \sqrt{\mu_i / \rho_i}$, that can be different in each domain. To alleviate the notation, we assume from now on that $f_1 = 0$ and $\rho_1 = \rho_2 = 1$; moreover, we define the normal fluxes on the interface Γ as follows:

$$\sigma_i := \sigma_i(u_i) := \mu_i \nabla u_i \cdot \mathrm{n}_i,$$

for $i = 1, 2$. First we impose a Neumann boundary condition on the boundary Γ_N of Ω:

$$\sigma_2(u_2) = \overline{\sigma}, \qquad \text{on } (0, T) \times \Gamma_N \tag{2}$$

where $\overline{\sigma}$ is a prescribed flux. Then we impose homogeneous initial conditions on Ω_i, $i = 1, 2$:

$$u_i(t = 0) = 0, \quad \dot{u}_i(t = 0) = 0. \tag{3}$$

Last but not least, the wave equations in each subdomain are coupled by the following transmission conditions for the unknowns and their fluxes on the interface Γ between domains Ω_1 and Ω_2:

$$u_1 = u_2, \qquad \sigma_1 + \sigma_2 = 0, \qquad \text{on } (0,T)\times\Gamma. \tag{4}$$

Remark. Instead of the condition $u_1 = u_2$, we can use alternatively a continuity condition that involves the time derivatives of the solutions:

$$\dot{u}_1 = \dot{u}_2 \qquad \text{on } (0,T)\times\Gamma. \tag{5}$$

2.2 Energetic BEM-FEM coupling

At first, the differential model problem in the unbounded domain Ω_1 is rewritten in terms of suitable space-time boundary integral equations over $(0,T)\times\Gamma$.

For D a domain in $\mathbb{R}^d$, $d = 1,2,3$, and V a vector space, we denote by $L^2(D;V)$ the Lebesgue space of V-valued square integrable functions. Similarly, we denote by $H^s(D;V)$ the Sobolev space of index s of V-valued functions, with $s \in \mathbb{R}$. When D is a space domain and $V = \mathbb{R}^m$, $m = 1,2,3$, we recover the usual Sobolev spaces [2, 30, 31]. When $m = 1$, we simply note $H^s(D)$ instead of $H^s(D;\mathbb{R})$. The usual scalar product of $H^s(D)$ is denoted by $(\cdot,\cdot)_{s,D}$ and the corresponding norm is denoted by $\|\cdot\|_{s,D}$. When $D = [0;T]$, with $T > 0$, and V is a Lebesgue or Sobolev space associated with a domain, we recover the usual Bochner spaces [19]. Let us introduce the standard inner products

$$< \cdot,\cdot >:=< \cdot,\cdot >_{L^2((0,T)\times\Omega_2)} \quad \text{and} \quad \langle\cdot,\cdot\rangle := \langle\cdot,\cdot\rangle_{L^2((0,T)\times\Gamma)}.$$

The latter can be also conceived as a duality product, for what concerns the space variable, between elements of $H^{\frac{1}{2}}(\Gamma)$ and $H^{-\frac{1}{2}}(\Gamma)$. Let $\mathcal{V}$, $\mathcal{K}$, $\mathcal{K}^*$, $\mathcal{D}$ be the usual integral operators defined as:

- $\mathcal{V} : L^2([0,T];H^{-\frac{1}{2}}(\Gamma)) \to H^1([0,T];H^{\frac{1}{2}}(\Gamma))$ such that

$$(\mathcal{V}\sigma_1)(\mathrm{x},t) = \int_0^t \int_{\Gamma_I} G(\mathrm{x},\mathrm{y};t,s)\sigma_1(\mathrm{y},s)\mathrm{d}\gamma_\mathrm{y}\mathrm{d}s;$$

- $\mathcal{K} : H^1([0,T];H^{\frac{1}{2}}(\Gamma)) \to H^1([0,T];H^{\frac{1}{2}}(\Gamma))$ such that

$$(\mathcal{K}u_1)(\mathrm{x},t) = \int_0^t \int_{\Gamma_I} \frac{\partial G}{\partial \mathbf{n}_{1,\mathrm{y}}}(\mathrm{x},\mathrm{y};t,s)u_1(\mathrm{y},s)\mathrm{d}\gamma_\mathrm{y}\mathrm{d}s;$$

- $\mathcal{K}^* : L^2([0,T];H^{-\frac{1}{2}}(\Gamma)) \to L^2([0,T];H^{-\frac{1}{2}}(\Gamma))$ such that

$$(\mathcal{K}^*\sigma_1)(\mathrm{x},t) = \int_0^t \int_{\Gamma_I} \frac{\partial G}{\partial \mathbf{n}_{1,\mathrm{x}}}(\mathrm{x},\mathrm{y};t,s)\sigma_1(\mathrm{y},s)\mathrm{d}\gamma_\mathrm{y}\mathrm{d}s;$$

- $\mathcal{D} : H^1([0,T];H^{\frac{1}{2}}(\Gamma)) \to L^2([0,T];H^{-\frac{1}{2}}(\Gamma))$ such that

$$(\mathcal{D}u_1)(\mathrm{x},t) = \int_0^t \int_{\Gamma_I} \frac{\partial^2 G}{\partial \mathbf{n}_{1,\mathrm{x}}\partial \mathbf{n}_{1,\mathrm{y}}}(\mathrm{x},\mathrm{y};t,s)u_1(\mathrm{y},s)\mathrm{d}\gamma_\mathrm{y}\mathrm{d}s.$$

The function G introduced above is defined as

$$G(\mathrm{x},\mathrm{y};t,s) := \frac{c_1}{2\pi\mu_1}\frac{H(c_1(t-s)-\|\mathrm{x}-\mathrm{y}\|_2)}{\sqrt{c_1^2(t-s)^2-\|\mathrm{x}-\mathrm{y}\|_2^2}},$$

and is the fundamental solution to the bi-dimensional wave equation (1), with $H(\cdot)$ the Heaviside step function. The integral formulation on $(0,T)\times\Gamma$ of the problem defined in $(0,T)\times\Omega_1$ is given by (see [3])

$$\begin{cases} \dfrac{1}{2}u_1(\mathrm{x},t) - \dfrac{1}{\mu_1}(\mathcal{V}\sigma_1)(\mathrm{x},t) + (\mathcal{K}u_1)(\mathrm{x},t) = 0, \\ -\dfrac{1}{2}\sigma_1(\mathrm{x},t) + (\mathcal{K}^*\sigma_1)(\mathrm{x},t) - \mu_1(\mathcal{D}u_1)(\mathrm{x},t) = 0. \end{cases} \tag{6}$$

At this stage, the just recalled integral model in $(0,T)\times\Omega_1$ and the differential model on $(0,T)\times\Omega_2$ are set in weak form, using energy considerations [3] and then coupled using the classical transmission conditions defined in the previous subsection. Having defined the following bilinear forms and linear functional:

- $B : [H^1([0,T];H^{\frac{1}{2}}(\Gamma)) \times L^2([0,T];H^{-\frac{1}{2}}(\Gamma))] \times [H^1([0,T];H^{\frac{1}{2}}(\Gamma)) \times L^2([0,T];H^{-\frac{1}{2}}(\Gamma))] \to \mathbb{R}$ such that

$$\begin{aligned} & B((u_1,\sigma_1),(v_1,\tau_1)) \qquad (7)\\ := \; & -\frac{1}{\mu_1}\langle(\dot{\mathcal{V}\sigma_1}),\tau_1\rangle + \langle(\frac{1}{2}\mathcal{I}+\dot{\mathcal{K}})u_1,\tau_1\rangle - \langle(\frac{1}{2}\mathcal{I}-\mathcal{K}^*)\sigma_1,\dot{v}_1\rangle - \mu_1\langle\mathcal{D}u_1,\dot{v}_1\rangle + \langle\sigma_1,\dot{v}_1\rangle \\ = \; & -\frac{1}{\mu_1}\langle(\dot{\mathcal{V}\sigma_1}),\tau_1\rangle + \langle(\frac{1}{2}\mathcal{I}+\dot{\mathcal{K}})u_1,\tau_1\rangle + \langle(\frac{1}{2}\mathcal{I}+\mathcal{K}^*)\sigma_1,\dot{v}_1\rangle - \mu_1\langle\mathcal{D}u_1,\dot{v}_1\rangle, \qquad (8)\end{aligned}$$

- $A : H^1([0,T];H^1(\Omega_2)) \times H^1([0,T];H^1(\Omega_2)) \to \mathbb{R}$ such that

$$A(u_2,v_2) := \mu_2 < \nabla u_2, \nabla\dot{v}_2 > + < \ddot{u}_2, \dot{v}_2 >,$$

- $F : H^1([0,T];H^1(\Omega_2)) \to \mathbb{R}$ such that

$$F(v_2) :=< f_2, \dot{v}_2 > + \langle\overline{\sigma}, \dot{v}_2\rangle_{L^2((0,T)\times\Gamma_N}\,,$$

the energetic BEM-FEM coupling reads:

find $u_2 \in H^1([0,T];H^1(\Omega_2))$ and $\sigma_1 \in H^0([0,T];H^{-\frac{1}{2}}(\Gamma))$ that solves

$$A(u_2,v_2) + B((u_2|_\Gamma,\sigma_1),(v_2|_\Gamma,\tau_1)) = F(v_2) \qquad (9)$$

for each $v_2 \in H^1([0,T];H^1(\Omega_2))$ and $\tau_1 \in H^0([0,T];H^{-\frac{1}{2}}(\Gamma))$.

In fact, the space-time boundary term coming from the energetic weak formulation of the differential model in $(0,T)\times\Omega_2$ is absorbed by the space-time bilinear form B, due to the fact that

$$-\langle\sigma_2(u_2),\dot{v}_2\rangle = \langle\sigma_1,\dot{v}_1\rangle.$$

This inner product has been simply added, as reported in (7), to the sum of the two space-time weak boundary integral equations, which is due to (6).

It is worth reporting now some energy estimates. Having introduced the energy of the solutions u_i, $i=1,2$, at time t as

$$\mathcal{E}_{\Omega_i}(u_i,t) := \frac{1}{2}\int_{\Omega_i}\big(\dot{u}_i^2(\mathrm{x},t) + \mu_i\|\nabla u_i(\mathrm{x},t)\|_2^2\big)\mathrm{dx}, \qquad (10)$$

it is straightforward to verify that, choosing the test functions $\tau_1=\sigma_1$ and $v_2=u_2$, it holds (see also [3])

$$A(u_2,u_2) = \mathcal{E}_{\Omega_2}(u_2,T) \quad \text{and} \quad B((u_1,\sigma_1),(u_1,\sigma_1)) = \langle\sigma_1,\dot{u}_1\rangle = \mathcal{E}_{\Omega_1}(u_1,T)\,. \qquad (11)$$

Hence the weak problem (9) gives

$$\mathcal{E}_{\Omega_1}(u_1,T) + \mathcal{E}_{\Omega_2}(u_2,T) = F(u_2). \qquad (12)$$

This allows us to derive *a priori* stability estimates for regular solutions u_1 and u_2, providing upper bounds for the associated energies in terms of the problem data. Indeed, assuming the the sake of simplicity $\overline{\sigma}(x,t)=0$, we can rewrite (12) as

$$\mathcal{E}_{\Omega_1}(u_1,T) + \mathcal{E}_{\Omega_2}(u_2,T) = \int_0^T\int_{\Omega_2}\dot{u}_2(\mathrm{x},t)f_2(\mathrm{x},t)d\mathrm{x}dt.$$

From this equality, by first applying Cauchy-Schwarz inequality and then Young's inequality, we get

$$\begin{aligned}\mathcal{E}_{\Omega_1}(u_1,T) + \mathcal{E}_{\Omega_2}(u_2,T) &\le \int_0^T ||\dot{u}_2(\cdot,t)||_{L^2(\Omega_2)}||f_2(\cdot,t)||_{L^2(\Omega_2)}\mathrm{d}t \\ &\le \frac{1}{2}\int_0^T ||\dot{u}_2(\cdot,t)||^2_{L^2(\Omega_2)}\mathrm{d}t + \frac{1}{2}\int_0^T ||f_2(\cdot,t)||^2_{L^2(\Omega_2)}\mathrm{d}t.\end{aligned}$$

Recalling the definition (10), we can write

$$\begin{aligned}\mathcal{E}_{\Omega_2}(u_2,T) &\leq \mathcal{E}_{\Omega_1}(u_1,T)+\mathcal{E}_{\Omega_2}(u_2,T)\\ &\leq \int_0^T \mathcal{E}_{\Omega_2}(u_2,t)dt+\frac{1}{2}\int_0^T ||f_2(\cdot,t)||^2_{L^2(\Omega_2)}\mathrm{d}t.\end{aligned}$$

From Gronwall's lemma, it follows that

$$\mathcal{E}_{\Omega_2}(u_2,T) \leq \frac{1}{2}\int_0^T ||f_2(\cdot,t)||^2_{L^2(\Omega_2)}\mathrm{d}t\ \exp(T), \tag{13}$$

i.e., an upper bound for $\mathcal{E}_{\Omega_2}(u_2,T)$. Using (13), we obtain an estimate as well for $\mathcal{E}_{\Omega_1}(u_1,T)$, in terms of the problem data:

$$\begin{aligned}\mathcal{E}_{\Omega_1}(u_1,T) &\leq \mathcal{E}_{\Omega_1}(u_1,T)+\mathcal{E}_{\Omega_2}(u_2,T)\\ &\leq \int_0^T \mathcal{E}_{\Omega_2}(u_2,t)dt+\frac{1}{2}\int_0^T ||f_2(\cdot,t)||^2_{L^2(\Omega_2)}\mathrm{d}t\\ &\leq \frac{1}{2}\int_0^T \left[\exp(t)\int_0^t ||f_2(\cdot,s)||^2_{L^2(\Omega_2)}\mathrm{d}s+||f_2(\cdot,t)||^2_{L^2(\Omega_2)}\right]\mathrm{d}t.\end{aligned} \tag{14}$$

2.3 Nitsche's approach

Our goal is to write a weak problem with Nitsche's treatment of the transmission conditions, similar to what has been introduced in [10] for elliptic problems. This time, we do not want to impose any strong restriction on the displacements or velocities, so there are no constraints on $\Gamma\times[0,T]$ for them. We can rewrite the strong coupling (9) as

$$A(u_2,v_2)-\langle\sigma_2(u_2),\dot{v}_2\rangle+B((u_1,\sigma_1),(v_1,\tau_1))-\langle\sigma_1,\dot{v}_1\rangle=F(v_2)$$

where now the inner products on $(0,T)\times\Gamma$ cannot simplify one another and we can start from the equality

$$\sigma_1+\sigma_2(u_2)=0 \quad \text{on } \Gamma_I\times[0,T] \tag{15}$$

to rewrite

$$\langle\sigma_2(u_2),\dot{v}_2\rangle+\langle\sigma_1,\dot{v}_1\rangle=\langle\sigma_2(u_2),\dot{v}_2-\dot{v}_1\rangle.$$

Then we impose weakly $\dot{u}_1=\dot{u}_2$, that we reformulate as

$$\chi\langle\dot{u}_2-\dot{u}_1,\dot{v}_2-\dot{v}_1\rangle=0, \qquad \text{with } \chi\in\mathbb{R}^+, \tag{16}$$

for each $v_2\in H^1([0,T];H^1(\Omega_2)), v_1\in H^1([0,T];H^{\frac{1}{2}}(\Gamma))$ and finally we introduce the term

$$\theta\langle\dot{u}_2-\dot{u}_1,\sigma_2(v_2)\rangle=0, \qquad \text{with } \theta\in\mathbb{R}, \tag{17}$$

for each $v_2\in H^1([0,T];H^1(\Omega_2))$, so that, as will be shown later, the energy estimates in the Nitsche's BEM-FEM case can be reduced to those of the simpler BEM-FEM case. Let us remark that the Nitsche's parameter χ is a quantity of dimension $space^{-1}$, as we will see later on, useful to still regard the left-hand side of (16) as a duality product in space variable. Moreover, the larger χ, the closer the weak imposition of continuity across the interface to the strong one.

After these preliminary steps, let us introduce a modified weak problem, that enables the coupling by Nitsche's approach, defined as:

find $\sigma_1\in H^0([0,T];H^{-\frac{1}{2}}(\Gamma))$, $u_1\in H^1([0,T];H^{\frac{1}{2}}(\Gamma))$, $u_2\in H^1([0,T];H^1(\Omega_2))$ solution to

$$A(u_2,v_2)-\langle\sigma_2(u_2),\dot{v}_2-\dot{v}_1\rangle-\theta\langle\dot{u}_2-\dot{u}_1,\sigma_2(v_2)\rangle+\chi\langle\dot{u}_2-\dot{u}_1,\dot{v}_2-\dot{v}_1\rangle+B((u_1,\sigma_1),(v_1,\tau_1))=F(v_2), \tag{18}$$

for each $\tau_1 \in H^0([0,T];H^{-\frac{1}{2}}(\Gamma))$, $v_1 \in H^1([0,T];H^{\frac{1}{2}}(\Gamma))$, $v_2 \in H^1([0,T];H^1(\Omega_2))$.

If we rewrite the weak problem (18) by choosing the test functions $\tau_1 = \sigma_1$, $v_1 = u_1$ and $v_2 = u_2$, by recalling (9)and (12), we get

$$\mathcal{E}_{\Omega_2}(u_2,T) - \langle \sigma_2(u_2), \dot{u}_2 - \dot{u}_1 \rangle - \theta \langle \dot{u}_2 - \dot{u}_1, \sigma_2(u_2) \rangle + \chi \langle \dot{u}_2 - \dot{u}_1, \dot{u}_2 - \dot{u}_1 \rangle + \mathcal{E}_{\Omega_1}(u_1,T) = F(u_2).$$

However, we can note that, due to (16) and (17), the terms multiplied by χ and θ vanish. Moreover, thanks to this particular choice of test functions, the term $\langle \sigma_2(u_2), \dot{u}_2 - \dot{u}_1 \rangle$ also vanishes due to (17). We thus recover the energy equality (12) also in the case of Nitsche's BEM-FEM coupling, and therefore the previous a priori stability estimates (13), (14) for the weak solutions still holds.

3 Approximation

For the time discretization, we define a uniform time grid $t_0 = 0, t_1, \ldots, t_{N-1}, t_N = T$ consisting of equally spaced instants. Setting $\Delta t = T/N$ with $N \in \mathbb{N}^+$, it is straightforward to see that

$$t_k := k\Delta t \qquad \text{with } k = 0, 1, \ldots, N.$$

We introduce a system $\{\bar{\psi}_0(t), \bar{\psi}_1(t), \ldots, \bar{\psi}_{N-1}(t)\}$ of linearly independent time functions such that

$$\bar{\psi}_k(t) = H(t - t_k) - H(t - t_{k+1}), \qquad k = 0, 1, \ldots, N-1$$

and a system $\{\widehat{\psi}_0(t), \widehat{\psi}_1(t), \ldots, \widehat{\psi}_{N-1}(t)\}$ of linearly independent time functions such that

$$\widehat{\psi}_k(t) = \frac{t - t_k}{\Delta t} H(t - t_k) - \frac{t - t_{k+1}}{\Delta t} H(t - t_{k+1}), \quad k = 0, 1, \ldots, N-1\,.$$

For the space discretization we consider a suitable polygonal approximation of Ω_2 and we denote by

$$\mathcal{T}^{(2)}_{\Delta x} := \{E_1, E_2, \ldots, E_{M_{\Delta x}}\}$$

an admissible triangular covering of Ω_2. The parameter $\Delta x > 0$ that characterizes the mesh $\mathcal{T}^{(2)}_{\Delta x}$ represents its characteristic size and allows to identify an important geometric constraint to be imposed on the triangles: for each $i = 1, 2, \ldots, M_{\Delta x}$, we shall assume that $\mathrm{diam}(E_i) < \Delta x$, where $\mathrm{diam}(E_i)$ is the diameter of E_i. Having defined M_2 as the number of vertices of the mesh $\mathcal{T}^{(2)}_{\Delta x}$, let us then consider a linearly independent Lagrangian system of piecewise linear functions in the space variable $\{\varphi_1(\mathrm{x}), \varphi_2(\mathrm{x}), \ldots, \varphi_{M_2}(\mathrm{x})\}$.

The restriction of the mesh $\mathcal{T}^{(2)}_{\Delta x}$ to the polygonal approximation of Γ defines a one-dimensional mesh $\mathcal{T}^{(2)}_{\widehat{\Delta x}} := \mathcal{T}^{(2)}_{\Delta x}|_\Gamma = \{e_1, e_2, \ldots, e_M\}$, consisting of M non-overlapping segments, whose characteristic parameter is defined by

$$\widehat{\Delta x} = \max_{1 \le i \le M} \mathrm{length}(e_i)\,.$$

Of course, we have that $\widehat{\Delta x} \le \Delta x$. Moreover, since each segment e_i can be identified by its endpoints, the number of nodes in $\mathcal{T}^{(2)}_{\widehat{\Delta x}}$ is equal to the number M of its elements.

On the same polygonal approximation of Γ we can define a different mesh $\mathcal{T}^{(1)}_{\widetilde{\Delta x}}$ of M_1 non-overlapping segments of maximum length $\widetilde{\Delta x}$ for the numerical approximation of the BEM solution related to the exterior unbounded domain Ω_1 and to complete the space discretization, we introduce on the interface Γ a linearly independent system of piecewise constant functions in the space variable $\{\bar{\varphi}_1(\mathrm{x}), \bar{\varphi}_2(\mathrm{x}), \ldots, \bar{\varphi}_{M_1}(\mathrm{x})\}$ and a linearly independent system of piecewise linear functions in the space variable $\{\widehat{\varphi}_1(\mathrm{x}), \widehat{\varphi}_2(\mathrm{x}), \ldots, \widehat{\varphi}_{M_1}(\mathrm{x})\}$.

We then introduce the following discrete spaces:

$$\mathcal{U}^{(2)}_{\Delta x, \Delta t} := \mathrm{span}\{\widehat{\psi}_k \varphi_j\} \quad \text{with } k = 0, 1, \ldots, N-1 \text{ and } j = 1, 2, \ldots, M_2,$$

$$\mathcal{U}^{(1)}_{\widetilde{\Delta x}, \Delta t} := \mathrm{span}\{\widehat{\psi}_k \hat{\varphi}_j\} \quad \text{with } k = 0, 1, \ldots, N-1 \text{ and } j = 1, 2, \ldots, M_1,$$

$$\mathcal{S}^{(1)}_{\widetilde{\Delta x},\Delta t} := \mathrm{span}\{\bar\psi_k\bar\varphi_j\} \quad \text{with } k=0,1,\dots,N-1 \text{ and } j=1,2,\dots,M_1,$$

which approximate the spaces $H^1([0,T];H^1(\Omega_2))$, $H^1([0,T];H^{\frac12}(\Gamma))$ and $L^2([0,T];H^{-\frac12}(\Gamma))$, respectively. We will search the approximate solutions of the Nitsche BEM-FEM coupling, namely:

$$u_2(\mathrm{x},t) \simeq u_2^*(\mathrm{x},t) := \sum_{k=0}^{N-1}\widehat\psi_k(t)\sum_{r=1}^{M_2}\alpha_{kr}\varphi_r(\mathrm{x}) =: \sum_{k=0}^{N-1}\widehat\psi_k(t)\Phi_k(\mathrm{x}), \tag{19}$$

$$u_1(\mathrm{x},t) \simeq u_1^*(\mathrm{x},t) := \sum_{k=0}^{N-1}\widehat\psi_k(t)\sum_{j=1}^{M_1}\widehat\alpha_{kj}\widehat\varphi_j(\mathrm{x}) =: \sum_{k=0}^{N-1}\widehat\psi_k(t)\widehat\Phi_k(\mathrm{x}) \tag{20}$$

$$\sigma_1(\mathrm{x},t) \simeq \sigma_1^*(\mathrm{x},t) := \sum_{k=0}^{N-1}\bar\psi_k(t)\sum_{\ell=1}^{M_1}\bar\alpha_{k\ell}\bar\varphi_\ell(\mathrm{x}) =: \sum_{k=0}^{N-1}\bar\psi_k(t)\bar\Phi_k(\mathrm{x}). \tag{21}$$

Hence, the discrete Nitsche BEM-FEM problem is obtained writing the weak coupled equation (18) in the above described approximation framework. We obtain

$$\begin{aligned} A(u_2^*,\widehat\psi_h\varphi_s) - \langle\sigma_2(u_2^*),\dot{\widehat\psi}_h\varphi_s - \dot{\widehat\psi}_h\hat\varphi_i\rangle + \chi\langle\dot u_2^* - \dot u_1^*,\dot{\widehat\psi}_h\varphi_s - \dot{\widehat\psi}_h\hat\varphi_i\rangle - \theta\langle\dot u_2^* - \dot u_1^*,\sigma_2(\widehat\psi_h\varphi_s)\rangle \\ + B((u_1^*,\sigma_1^*),(\widehat\psi_h\hat\varphi_i,\bar\psi_h\bar\varphi_m)) = F(\widehat\psi_h\varphi_s), \end{aligned} \tag{22}$$

for $h=0,\cdots,N-1$, $s=1,\cdots,M_2$, $i,m=1,\cdots,M_1$, which is equivalent to a linear system

$$\mathbb{E}\alpha = \mathrm{f}\,, \tag{23}$$

in the $N(M_2+2M_1)$ unknowns $\alpha=(\alpha_k)_{k=0,\cdots,N-1}$, where

$$\alpha_k = (\alpha_{k1},\cdots,\alpha_{kM_2},\widehat\alpha_{k1},\cdots,\widehat\alpha_{kM_1},\bar\alpha_{k1},\cdots,\bar\alpha_{kM_1},$$

with $\mathrm{f}=(\mathrm{f}_h)_{h=0,\cdots,N-1}$ where $\mathrm{f}_h=(\mathrm{f}_{h1},\cdots,\mathrm{f}_{hM_2},0)$, being 0 a trivial vector of length $2M_1$.
Substituting (19)-(21) into (22), this latter can be specified as

$$\begin{aligned} &\sum_{k=0}^{N-1}\Bigg[\sum_{r=1}^{M_2}\alpha_{kr}\Big(\rho_{hk}p_{sr}+\zeta_{hk}q_{sr}\Big) - \sum_{r=1}^{M_2}\alpha_{kr}\Big(\rho_{hk}s^1_{sr}-\rho_{hk}s^2_{ir}\Big) \\ &+\chi\sum_{r=1}^{M_2}\alpha_{kr}\Big(\varsigma_{hk}g^1_{sr}-\varsigma_{hk}g^2_{ir}\Big) - \chi\sum_{j=1}^{M_1}\widehat\alpha_{kj}\Big(\varsigma_{hk}g^3_{sj}-\varsigma_{hk}g^4_{ij}\Big) - \theta\sum_{r=1}^{M_2}\alpha_{kr}\tilde\rho_{hk}t^1_{sr} + \theta\sum_{j=1}^{M_1}\widehat\alpha_{kj}\tilde\rho_{hk}t^2_{sj} \\ &-\sum_{\ell=1}^{M_1}\bar\alpha_{k\ell}v^{k\ell}_{hm} + \sum_{j=1}^{M_1}\widehat\alpha_{kj}\Big(\frac12\delta_{hk}c_{mj}+k^{kj}_{hm}\Big) + \sum_{\ell=1}^{M_1}\bar\alpha_{k\ell}\Big(\frac12\delta_{hk}\tilde c_{i\ell}+k^{*k\ell}_{hi}\Big) - \sum_{j=1}^{M_1}\widehat\alpha_{kj}d^{kj}_{hi}\Bigg] = \mathrm{f}_{hs}\,, \end{aligned} \tag{24}$$

where, for $k,h=0,1,\dots,N-1$, $r,s=1,2,\dots,M_2$, $j,i,\ell,m=1,2,\dots,M_1$, we have introduced the following notation, where δ_{hk} is the Kronecker symbol:

$$\rho_{hk} := \begin{cases} 1/2, & h=k \\ 1, & h>k \\ 0, & h<k \end{cases}, \qquad \zeta_{hk} := \frac{1}{\Delta t^2}\begin{cases} 1, & h=k \\ -1, & h=k+1 \\ 0, & h\neq k,k+1 \end{cases}, \qquad \varsigma_{hk} := \frac{1}{\Delta t}\delta_{hk}, \qquad \tilde\rho_{hk} := \rho_{kh}$$

as well as

$$
\begin{aligned}
q_{sr} &:= (\varphi_s, \varphi_r)_{L^2(\Omega_2)}, & p_{sr} &:= \mu_2(\nabla\varphi_s, \nabla\varphi_r)_{L^2(\Omega_2)},\\
s^1_{sr} &:= (\sigma_2(\varphi_r), \varphi_s)_{L^2(\Gamma)}, & s^2_{ir} &:= (\sigma_2(\varphi_r), \widehat{\varphi}_i)_{L^2(\Gamma)},\\
g^1_{sr} &:= (\varphi_r, \varphi_s)_{L^2(\Gamma)}, & g^2_{ir} &:= (\varphi_r, \widehat{\varphi}_i)_{L^2(\Gamma)},\\
g^3_{sj} &:= (\widehat{\varphi}_j, \varphi_s)_{L^2(\Gamma)}, & g^4_{ij} &:= (\widehat{\varphi}_j, \widehat{\varphi}_i)_{L^2(\Gamma)}\\
t^1_{sr} &:= (\varphi_r, \sigma_2(\varphi_s))_{L^2(\Gamma)}, & t^2_{sj} &:= (\widehat{\varphi}_j, \sigma_2(\varphi_s))_{L^2(\Gamma)},\\
c_{mj} &:= (\widehat{\varphi}_j, \bar{\varphi}_m)_{L^2(\Gamma)}, & \tilde{c}_{il} &= c_{li},\\
v^{k\ell}_{hm} &:= \frac{1}{\mu_1}\langle \mathcal{V}(\dot{\bar{\psi}}_k\bar{\varphi}_\ell), \bar{\psi}_h\bar{\varphi}_m\rangle, & k^{kj}_{hm} &:= \langle \mathcal{K}(\dot{\widehat{\psi}}_k\hat{\varphi}_j), \bar{\psi}_h\bar{\varphi}_m\rangle,\\
k^{*k\ell}_{hi} &:= \langle \mathcal{K}^*(\bar{\psi}_k\bar{\varphi}_\ell), \dot{\hat{\psi}}_h\hat{\varphi}_i\rangle, & d^{kj}_{hi} &:= \mu_1\langle \mathcal{D}(\widehat{\psi}_k\widehat{\varphi}_j), \dot{\hat{\psi}}_h\hat{\varphi}_i\rangle,
\end{aligned}
$$

and finally

$$
\mathrm{f}_{hs} := < f_2, \dot{\widehat{\psi}}_h\varphi_s > + \langle \overline{\sigma}, \dot{\widehat{\psi}}_h\varphi_s\rangle_{L^2((0,T)\times\Gamma_N}.
$$

The interested reader is referred to [3] for more details about BEM matrix entries.
Let us now remark that the energetic BEM-FEM coupling is algebraically reformulated as a linear system whose matrix presents a block lower triangular Toeplitz structure, which is extremely important for an efficient storage and the use of block forward substitution algorithm. Unfortunately, this matrix structure is not maintained by the Nitsche's coupling approach, except for the non-symmetric variant $\theta = 0$. In this case, if we denote by $\mathbb{E}^{(\ell)}$ the block obtained when $t_h - t_k = \ell\Delta t$, $\ell = 0, 1, \ldots, N-1$, the linear system (24) can be written as

$$
\begin{pmatrix}
\mathbb{E}^{(0)} & 0 & 0 & \cdots & 0\\
\mathbb{E}^{(1)} & \mathbb{E}^{(0)} & 0 & \cdots & 0\\
\mathbb{E}^{(2)} & \mathbb{E}^{(1)} & \mathbb{E}^{(0)} & \cdots & 0\\
\vdots & \vdots & \vdots & \ddots & \vdots\\
\mathbb{E}^{(N-1)} & \mathbb{E}^{(N-2)} & \mathbb{E}^{(N-3)} & \cdots & \mathbb{E}^{(0)}
\end{pmatrix}
\begin{pmatrix}
\alpha^{(0)}\\ \alpha^{(1)}\\ \alpha^{(2)}\\ \vdots\\ \alpha^{(N-1)}
\end{pmatrix}
=
\begin{pmatrix}
\mathrm{f}^{(0)}\\ \mathrm{f}^{(1)}\\ \mathrm{f}^{(2)}\\ \vdots\\ \mathrm{f}^{(N-1)}
\end{pmatrix}
$$

where

$$
\mathbb{E}^{(0)} := \begin{pmatrix}
\frac{1}{2}P + \frac{1}{\Delta t^2}Q - \frac{1}{2}S_1 + \frac{\chi}{\Delta t}G_1 & O & -\frac{\chi}{\Delta t}G_3\\
O & -V^{(0)} & \frac{1}{2}C + K^{(0)}\\
\frac{1}{2}S_2 - \frac{\chi}{\Delta t}G_2 & \frac{1}{2}\tilde{C} + K^{*(0)} & \frac{\chi}{\Delta t}G_4 - D^{(0)}
\end{pmatrix},
$$

and

$$
\mathbb{E}^{(1)} := \begin{pmatrix}
P - \frac{1}{\Delta t^2}Q - S_1 & O & O\\
O & -V^{(1)} & K^{(1)}\\
S_2 & K^{*(1)} & -D^{(1)}
\end{pmatrix},
$$

whereas for $\ell = 2, \ldots, N-1$ we have

$$
\mathbb{E}^{(\ell)} = \begin{pmatrix}
P - S_1 & O & O\\
O & -V^{(\ell)} & K^{(\ell)}\\
S_2 & K^{*(\ell)} & -D^{(\ell)}
\end{pmatrix}.
$$

Numerical results given in Section 5 have been obtained under the choice $\theta = 0$.

4 Discrete energy estimates

To derive discrete energy estimates, assuming again for the sake of simplicity $\bar{\sigma}(\mathrm{x}, t) = 0$ and remembering the definition of the bilinear form B, we can rewrite (18) as

$$
A(u_2, v_2) - \langle \sigma_2(u_2), \dot{v}_2 - \dot{v}_1\rangle + \chi\langle \dot{u}_2 - \dot{u}_1, \dot{v}_2 - \dot{v}_1\rangle - \theta\langle \dot{u}_2 - \dot{u}_1, \sigma_2(v_2)\rangle + \langle \sigma_1, \dot{v}_1\rangle = F(v_2). \tag{25}
$$

Using the approximate solutions (19)-(21) and choosing as test functions

$$v_2^*(x,t) = \widehat{\psi}_h(t)\Phi_h(x), \quad v_1^*(x,t) = \widehat{\psi}_h(t)\widehat{\Phi}_h(x),$$

to be later summed over $h = 0, \cdots, N-1$, we are going to rewrite all the terms in equation (25) in the considered discrete framework, considering also the choice

$$\chi = \frac{\chi_0}{\Delta x}\,, \tag{26}$$

as it is standard in Nitsche's coupling for elliptic problems [10] (see also [9, 33, 38]). The definitions of the two temporal bases used to construct the discrete functional spaces $\mathcal{U}^{(2)}_{\Delta x,\Delta t}$, $\mathcal{U}^{(1)}_{\widetilde{\Delta x},\Delta t}$ and $\mathcal{S}^{(1)}_{\widetilde{\Delta x},\Delta t}$ imply that

$$u_2^*(\mathrm{x},t_h) = \sum_{k=0}^{N-1} \widehat{\psi}_k(t_h)\Phi_k(\mathrm{x}) = \sum_{k=0}^{h-1} \Phi_k(\mathrm{x}) =: u_2^h,$$

$$u_1^*(\mathrm{x},t_h) = \sum_{k=0}^{N-1} \widehat{\psi}_k(t_h)\widehat{\Phi}_k(\mathrm{x}) = \sum_{k=0}^{h-1} \widehat{\Phi}_k(\mathrm{x}) =: u_1^h,$$

$$\sigma_1^*(\mathrm{x},t_h) = \sum_{k=0}^{N-1} \bar{\psi}_k(t_h)\bar{\Phi}_k(x) = \bar{\Phi}_h(\mathrm{x}) =: \sigma_1^h.$$

This yields

$$\Phi_h(\mathrm{x}) = \Phi_h(\mathrm{x}) + \sum_{k=0}^{h-1} \Phi_k(\mathrm{x}) - \sum_{k=0}^{h-1} \Phi_k(\mathrm{x}) = \sum_{k=0}^{h} \Phi_k(\mathrm{x}) - \sum_{k=0}^{h-1} \Phi_k(\mathrm{x}) = u_2^{h+1} - u_2^h,$$

$$\widehat{\Phi}_h(\mathrm{x}) = \widehat{\Phi}_h(\mathrm{x}) + \sum_{k=0}^{h-1} \widehat{\Phi}_k(\mathrm{x}) - \sum_{k=0}^{h-1} \widehat{\Phi}_k(\mathrm{x}) = \sum_{k=0}^{h} \widehat{\Phi}_k(\mathrm{x}) - \sum_{k=0}^{h-1} \widehat{\Phi}_k(\mathrm{x}) = u_1^{h+1} - u_1^h.$$

We start from the first term on the left-hand side of (25) and, thanks to the definition of the bilinear form A, separating space and time integrals and evaluating these latter analytically, we obtain the following:

$$\begin{aligned}
A(u_2^*, v_2^*) &= A\left(\sum_{k=0}^{N-1} \widehat{\psi}_k\Phi_k, \widehat{\psi}_h\Phi_h\right) = \sum_{k=0}^{N-1} A(\widehat{\psi}_k\Phi_k, \widehat{\psi}_h\Phi_h) \\
&= \sum_{k=0}^{N-1} \left[\mu_2 < \widehat{\psi}_k\nabla\Phi_k, \dot{\widehat{\psi}}_h\nabla\Phi_h > + < \ddot{\widehat{\psi}}_k\Phi_k, \dot{\widehat{\psi}}_h\Phi_h >\right] \\
&= \frac{\mu_2}{2}(\nabla\Phi_h, \nabla\Phi_h)_{L^2(\Omega_2)} + \mu_2 \sum_{k=0}^{h-1}(\nabla\Phi_k, \nabla\Phi_h)_{L^2(\Omega_2)} + \left(\Phi_h, \frac{\Phi_h - \Phi_{h-1}}{\Delta t^2}\right)_{L^2(\Omega_2)} \qquad (27) \\
&= \frac{\mu_2}{2}(\nabla(u_2^{h+1} - u_2^h), \nabla(u_2^{h+1} - u_2^h))_{L^2(\Omega_2)} + \mu_2(\nabla u_2^h, \nabla(u_2^{h+1} - u_2^h))_{L^2(\Omega_2)} \\
&\quad + \left(u_2^{h+1} - u_2^h, \frac{u_2^{h+1} - 2u_2^h + u_2^{h-1}}{\Delta t^2}\right)_{L^2(\Omega_2)} \\
&= \mu_2\left(\frac{\nabla(u_2^{h+1} + u_2^h)}{2}, \nabla(u_2^{h+1} - u_2^h)\right)_{L^2(\Omega_2)} + \left(u_2^{h+1} - u_2^h, \frac{u_2^{h+1} - 2u_2^h + u_2^{h-1}}{\Delta t^2}\right)_{L^2(\Omega_2)} \\
&= \frac{\mu_2}{2}\left(||\nabla u_2^{h+1}||^2_{L^2(\Omega_2)} - ||\nabla u_2^h||^2_{L^2(\Omega_2)}\right) + \left(u_2^{h+1} - u_2^h, \frac{u_2^{h+1} - 2u_2^h + u_2^{h-1}}{\Delta t^2}\right)_{L^2(\Omega_2)}. \qquad (28)
\end{aligned}$$

Similar steps can be carried out for all the terms in (25). Hence, for the second term on the left-hand side, up to the sign, we get

$$\begin{aligned}
&\langle \sigma_2(u_2^*), \dot{v}_2^* - \dot{v}_1^* \rangle = \sum_{k=0}^{N-1} \langle \widehat{\psi}_k \sigma_2(\Phi_k), \dot{\widehat{\psi}}_h \Phi_h - \dot{\widehat{\psi}}_h \widehat{\Phi}_h \rangle \\
&= \frac{1}{2}(\sigma_2(\Phi_h), \Phi_h - \widehat{\Phi}_h)_{L^2(\Gamma)} + \sum_{k=0}^{h-1} (\sigma_2(\Phi_k), \Phi_h - \widehat{\Phi}_h)_{L^2(\Gamma)} \\
&= \frac{1}{2}(\sigma_2(u_2^{h+1} - u_2^h), (u_2^{h+1} - u_2^h) - (u_1^{h+1} - u_1^h))_{L^2(\Gamma)} + (\sigma_2(u_2^h), (u_2^{h+1} - u_2^h) - (u_1^{h+1} - u_1^h))_{L^2(\Gamma)} \\
&= \frac{1}{2}(\sigma_2(u_2^{h+1}) + \sigma_2(u_2^h), (u_2^{h+1} - u_2^h) - (u_1^{h+1} - u_1^h))_{L^2(\Gamma)}.
\end{aligned}$$

Regarding the third term, we obtain

$$\begin{aligned}
&\frac{\chi_0}{\Delta x}\langle \dot{u}_2^* - \dot{u}_1^*, \dot{v}_2^* - \dot{v}_1^* \rangle = \frac{\chi_0}{\Delta x} \sum_{k=0}^{N-1} \langle \dot{\widehat{\psi}}_k \Phi_k - \dot{\widehat{\psi}}_k \widehat{\Phi}_k, \dot{\widehat{\psi}}_h \Phi_h - \dot{\widehat{\psi}}_h \widehat{\Phi}_h \rangle \\
&= \frac{\chi_0}{\Delta x \Delta t}(\Phi_h, \Phi_h - \widehat{\Phi}_h)_{L^2(\Gamma)} - \frac{\chi_0}{\Delta x \Delta t}(\widehat{\Phi}_h, \Phi_h - \widehat{\Phi}_h)_{L^2(\Gamma)} \\
&= \frac{\chi_0}{\Delta x \Delta t}\left[||u_2^{h+1} - u_2^h||^2_{L^2(\Gamma)} - 2(u_2^{h+1} - u_2^h, u_1^{h+1} - u_1^h)_{L^2(\Gamma)} + ||u_1^{h+1} - u_1^h||^2_{L^2(\Gamma)} \right] \\
&= \frac{\chi_0}{\Delta x \Delta t} \left\| (u_2^{h+1} - u_2^h) - (u_1^{h+1} - u_1^h) \right\|^2_{L^2(\Gamma)} .
\end{aligned}$$

The fourth term, up to the sign, is treated as follows

$$\begin{aligned}
&\theta \langle \dot{u}_2^* - \dot{u}_1^*, \sigma_2(v_2^*) \rangle = \theta \sum_{k=0}^{N-1} \langle \dot{\widehat{\psi}}_k \Phi_k - \dot{\widehat{\psi}}_k \widehat{\Phi}_k, \widehat{\psi}_h \sigma_2(\Phi_h) \rangle \\
&= \frac{\theta}{2}(\Phi_h - \widehat{\Phi}_h, \sigma_2(\Phi_h))_{L^2(\Gamma)} + \theta \sum_{k=h+1}^{N-1} (\Phi_k - \widehat{\Phi}_k, \sigma_2(\Phi_h))_{L^2(\Gamma)} \\
&= \theta \left(\left(u_2^N - \frac{u_2^{h+1} + u_2^h}{2} \right) - \left(u_1^N - \frac{u_1^{h+1} + u_1^h}{2} \right), \sigma_2(u_2^{h+1} - u_2^h) \right)_{L^2(\Gamma)} .
\end{aligned}$$

Since in the end we are going to sum over the index $h = 0, \cdots, N-1$, it is not difficult to prove, with a straightforward but cumbersome computation (which we skip), that the sum is equal to the sum of

$$\frac{\theta}{2}(\sigma_2(u_2^{h+1}) + \sigma_2(u_2^h), (u_2^{h+1} - u_2^h) - (u_1^{h+1} - u_1^h))_{L^2(\Gamma)}.$$

This term coincides, up to θ coefficient, with the second term above.

For the last term on the left-hand side of (25), we write

$$\langle \sigma_1^*, \dot{v}_1^* \rangle = \sum_{k=0}^{N-1} \langle \bar{\psi}_k \bar{\Phi}_k, \dot{\hat{\psi}}_h \hat{\Phi}_h \rangle = (\bar{\Phi}_h, \widehat{\Phi}_h)_{L^2(\Gamma)} = (\sigma_1^h, u_1^{h+1} - u_1^h)_{L^2(\Gamma)} .$$

For the right-hand side, we obtain

$$F(v_2^*) = F(\widehat{\psi}_h \Phi_h) = (\Phi_h, F_h)_{L^2(\Omega_2)} = (u_2^{h+1} - u_2^h, F_h)_{L^2(\Omega_2)}$$

with

$$F_h(\mathrm{x}) := \int_0^T \dot{\widehat{\psi}}_h(t) f_2(\mathrm{x}, t) \mathrm{d}t.$$

At this stage, the weak problem (25) can be rewritten as follows:

$$\begin{aligned}
&\frac{\mu_2}{2}\left(||\nabla u_2^{h+1}||^2_{L^2(\Omega_2)} - ||\nabla u_2^h||^2_{L^2(\Omega_2)}\right) + \frac{1}{\Delta t^2}\left(u_2^{h+1}-u_2^h, u_2^{h+1}-2u_2^h+u_2^{h-1}\right)_{L^2(\Omega_2)}\\
&-\frac{(1+\theta)}{2}\left(\sigma_2(u_2^{h+1})+\sigma_2(u_2^h),(u_2^{h+1}-u_2^h)-(u_1^{h+1}-u_1^h)\right)_{L^2(\Gamma)}\\
&+\frac{\chi_0}{\Delta x\Delta t}\left\|(u_2^{h+1}-u_2^h)-(u_1^{h+1}-u_1^h)\right\|^2_{L^2(\Gamma)} + \left(\sigma_1^h, u_1^{h+1}-u_1^h\right)_{L^2(\Gamma)} = \left(u_2^{h+1}-u_2^h, F_h\right)_{L^2(\Omega_2)}. \qquad (29)
\end{aligned}$$

Before summing over $h = 0, \cdots, N-1$, we give lower bounds for the second and third terms in (29).

At first, we focus on the quantity

$$\begin{aligned}
&\left(u_2^{h+1}-u_2^h, u_2^{h+1}-2u_2^h+u_2^{h-1}\right)_{L^2(\Omega_2)} = \left(u_2^{h+1}-u_2^h, (u_2^{h+1}-u_2^h)-(u_2^h-u_2^{h-1})\right)_{L^2(\Omega_2)}\\
&= \left\|u_2^{h+1}-u_2^h\right\|^2_{L^2(\Omega_2)} - \left(u_2^{h+1}-u_2^h, u_2^h-u_2^{h-1}\right)_{L^2(\Omega_2)}.
\end{aligned}$$

By applying Young's inequality, we get

$$\begin{aligned}
&\left(u_2^{h+1}-u_2^h, u_2^{h+1}-2u_2^h+u_2^{h-1}\right)_{L^2(\Omega_2)}\\
&\geq \left\|u_2^{h+1}-u_2^h\right\|^2_{L^2(\Omega_2)} - \frac{1}{2}\left\|u_2^{h+1}-u_2^h\right\|^2_{L^2(\Omega_2)} - \frac{1}{2}\left\|u_2^h-u_2^{h-1}\right\|^2_{L^2(\Omega_2)}\\
&= \frac{1}{2}\left\|u_2^{h+1}-u_2^h\right\|^2_{L^2(\Omega_2)} - \frac{1}{2}\left\|u_2^h-u_2^{h-1}\right\|^2_{L^2(\Omega_2)}.
\end{aligned}$$

Using this result, we obtain a lower bound for the second term on the left-hand side of (29), leading to the following inequality

$$\begin{aligned}
&\frac{\mu_2}{2}\left(||\nabla u_2^{h+1}||^2_{L^2(\Omega_2)} - ||\nabla u_2^h||^2_{L^2(\Omega_2)}\right) + \frac{1}{2\Delta t^2}\left(||u_2^{h+1}-u_2^h||^2_{L^2(\Omega_2)} - ||u_2^h-u_2^{h-1}||^2_{L^2(\Omega_2)}\right)\\
&-\frac{(1+\theta)}{2}\left(\sigma_2(u_2^{h+1})+\sigma_2(u_2^h),(u_2^{h+1}-u_2^h)-(u_1^{h+1}-u_1^h)\right)_{L^2(\Gamma)}\\
&+\frac{\chi_0}{\Delta x\Delta t}\|(u_2^{h+1}-u_2^h)-(u_1^{h+1}-u_1^h)\|^2_{L^2(\Gamma)} + \left(\sigma_1^h, u_1^{h+1}-u_1^h\right)_{L^2(\Gamma)} \leq \left(u_2^{h+1}-u_2^h, F_h\right)_{L^2(\Omega_2)}. \qquad (30)
\end{aligned}$$

Introducing now the discrete energies so that they reflect the definition given in the continuous formulation (10), i.e.

$$\mathcal{E}_i^{h+1} := \frac{1}{2}\left\|\frac{u_i^{h+1}-u_i^h}{\Delta t}\right\|^2_{L^2(\Omega_i)} + \frac{\mu_i}{2}||\nabla u_i^{h+1}||^2_{L^2(\Omega_i)}, \quad i=1,2, \quad h=0,\cdots,N-1,$$

we can rewrite (30) as:

$$\begin{aligned}
&\mathcal{E}_2^{h+1}-\mathcal{E}_2^h - \frac{(1+\theta)}{2}\left(\sigma_2(u_2^{h+1})+\sigma_2(u_2^h),(u_2^{h+1}-u_2^h)-(u_1^{h+1}-u_1^h)\right)_{L^2(\Gamma)}\\
&+\frac{\chi_0}{\Delta x\Delta t}||(u_2^{h+1}-u_2^h)-(u_1^{h+1}-u_1^h)||^2_{L^2(\Gamma)} + \left(\sigma_1^h, u_1^{h+1}-u_1^h\right)_{L^2(\Gamma)} \leq \left(u_2^{h+1}-u_2^h, F_h\right)_{L^2(\Omega_2)}. \qquad (31)
\end{aligned}$$

Let us now focus on the third term, which, up to the sign, can be split into the sum of

$$\Theta_\ell := \frac{(1+\theta)}{2}\left(\sigma_2(u_2^\ell),(u_2^{h+1}-u_2^h)-(u_1^{h+1}-u_1^h)\right)_{L^2(\Gamma)}, \quad \text{for} \qquad \ell = h, h+1.$$

We have the following chain, obtained using Cauchy-Schwarz and discrete trace inequalities in space variable (the latter based on the local trace inequality, see, *e.g.*, [39, Lemma 2.1], over each triangular element of $\mathcal{T}^{(2)}_{\Delta x}$), being C a suitable real and positive constant independent of the discretization parameters:

$$\begin{aligned}
\Theta_\ell &\leq \frac{1}{2}\|\sigma_2(u_2^\ell)\|_{L^2(\Gamma)}\,|1+\theta|\|(u_2^{h+1}-u_2^h)-(u_1^{h+1}-u_1^h)\|_{L^2(\Gamma)}\\
&\leq \frac{1}{2}C\Delta x^{-\frac{1}{2}}\mu_2\|\nabla u_2^\ell\|_{L^2(\Omega_2)}\,|1+\theta|\|(u_2^{h+1}-u_2^h)-(u_1^{h+1}-u_1^h)\|_{L^2(\Gamma)}
\end{aligned}$$

and we continue estimating from above, using Young's inequalities, with different coefficients for $\ell = h$ and $\ell = h+1$, namely:

$$\begin{aligned}\Theta_h &\leq \Delta t \frac{\mu_2}{4}\|\nabla u_2^h\|^2_{L^2(\Omega_2)} + \frac{(1+\theta)^2C^2\mu_2}{4\Delta x\Delta t}\|(u_2^{h+1}-u_2^h)-(u_1^{h+1}-u_1^h)\|^2_{L^2(\Gamma)}\\ &\leq \frac{\Delta t}{2}\mathcal{E}_2^h + \frac{(1+\theta)^2C^2\mu_2}{4\Delta x\Delta t}\|(u_2^{h+1}-u_2^h)-(u_1^{h+1}-u_1^h)\|^2_{L^2(\Gamma)},\end{aligned}$$

for $\ell = h$, and

$$\begin{aligned}\Theta_{h+1} &\leq \Delta t \frac{\mu_2}{8}\|\nabla u_2^{h+1}\|^2_{L^2(\Omega_2)} + \frac{(1+\theta)^2C^2\mu_2}{2\Delta x\Delta t}\|(u_2^{h+1}-u_2^h)-(u_1^{h+1}-u_1^h)\|^2_{L^2(\Gamma)}\\ &\leq \frac{\Delta t}{4}\mathcal{E}_2^{h+1} + \frac{(1+\theta)^2C^2\mu_2}{2\Delta x\Delta t}\|(u_2^{h+1}-u_2^h)-(u_1^{h+1}-u_1^h)\|^2_{L^2(\Gamma)},\end{aligned}$$

for $\ell = h+1$, obtaining finally the following estimate for the third term in (31):

$$\begin{aligned}&\frac{(1+\theta)}{2}\left(\sigma_2(u_2^{h+1})+\sigma_2(u_2^h),(u_2^{h+1}-u_2^h)-(u_1^{h+1}-u_1^h)\right)_{L^2(\Gamma)}\\ \leq\ &\frac{\Delta t}{2}\mathcal{E}_2^h + \frac{\Delta t}{4}\mathcal{E}_2^{h+1} + \frac{3(1+\theta)^2C^2\mu_2}{4\Delta x\Delta t}\|(u_2^{h+1}-u_2^h)-(u_1^{h+1}-u_1^h)\|^2_{L^2(\Gamma)}.\end{aligned}$$

Inserting this inequality into (31) we obtain

$$\begin{aligned}&\mathcal{E}_2^{h+1}-\mathcal{E}_2^h-\frac{\Delta t}{4}\mathcal{E}_2^{h+1}-\frac{\Delta t}{2}\mathcal{E}_2^h+\frac{4\chi_0-3(1+\theta)^2C^2\mu_2}{4\Delta x\Delta t}\|(u_2^{h+1}-u_2^h)-(u_1^{h+1}-u_1^h)\|^2_{L^2(\Gamma)}\\ &+\left(\sigma_1^h,u_1^{h+1}-u_1^h\right)_{L^2(\Gamma)} \leq \left(u_2^{h+1}-u_2^h,F_h\right)_{L^2(\Omega_2)}.\end{aligned} \tag{32}$$

Having fixed $\theta \in \mathbb{R}$, for $\chi_0 \in \mathbb{R}^+$ sufficiently large, i.e.

$$\chi_0 > \frac{3}{4}(1+\theta)^2C^2\mu_2$$

and applying the Cauchy–Schwarz inequality to bound the right-hand side, we obtain

$$\begin{aligned}&\mathcal{E}_2^{h+1}-\mathcal{E}_2^h-\frac{\Delta t}{2}\mathcal{E}_2^h-\frac{\Delta t}{4}\mathcal{E}_2^{h+1}+\left(\sigma_1^h,u_1^{h+1}-u_1^h\right)_{L^2(\Gamma)}\\ \leq\ &||u_2^{h+1}-u_2^h||_{L^2(\Omega_2)}||F_h||_{L^2(\Omega_2)} = \Delta t\left\|\frac{u_2^{h+1}-u_2^h}{\Delta t}\right\|_{L^2(\Omega_2)}||F_h||_{L^2(\Omega_2)}.\end{aligned}$$

Using Young's inequality once more, we get

$$\begin{aligned}&\mathcal{E}_2^{h+1}-\mathcal{E}_2^h-\frac{\Delta t}{2}\mathcal{E}_2^h-\frac{\Delta t}{4}\mathcal{E}_2^{h+1}+\left(\sigma_1^h,u_1^{h+1}-u_1^h\right)_{L^2(\Gamma)}\\ \leq\ &\Delta t\left(\frac{1}{8}\left\|\frac{u_2^{h+1}-u_2^h}{\Delta t}\right\|^2_{L^2(\Omega_2)}+2||F_h||^2_{L^2(\Omega_2)}\right) \leq \frac{\Delta t}{4}\mathcal{E}_2^{h+1}+2\Delta t||F_h||^2_{L^2(\Omega_2)}.\end{aligned}$$

This yields:

$$\mathcal{E}_2^{h+1}-\mathcal{E}_2^h+\left(\sigma_1^h,u_1^{h+1}-u_1^h\right)_{L^2(\Gamma)} \leq \frac{\Delta t}{2}\mathcal{E}_2^{h+1}+\frac{\Delta t}{2}\mathcal{E}_2^h+2\Delta t||F_h||^2_{L^2(\Omega_2)}.$$

Summing now over the index h varying from 0 to $N-1$ and noting that $\mathcal{E}_2^0 = 0$, we see that

$$\mathcal{E}_2^N+\Delta t\sum_{h=0}^{N-1}\left(\sigma_1^h,\frac{u_1^{h+1}-u_1^h}{\Delta t}\right)_{L^2(\Gamma)} \leq \frac{\Delta t}{2}\mathcal{E}_2^N+\Delta t\sum_{h=0}^{N-1}\mathcal{E}_2^h+2\Delta t\sum_{h=0}^{N-1}||F_h||^2_{L^2(\Omega_2)}. \tag{33}$$

Considering the second term on the left-hand side of (33) as an iterated one-point quadrature formula we observe that

$$\Delta t \sum_{h=0}^{N-1} \left(\sigma_1^h, \frac{u_1^{h+1} - u_1^h}{\Delta t} \right)_{L^2(\Gamma)} \simeq \langle \sigma_1, \dot{u}_1 \rangle \tag{34}$$

and therefore, remembering (11), the left-hand side of (34) represents the approximate energy of the BEM subdomain at the final time instant of analysis, i.e. $\mathcal{E}_1^N$. Substituting this value into (33), we obtain

$$\left(1 - \frac{\Delta t}{2}\right) \mathcal{E}_2^N + \mathcal{E}_1^N \leq \Delta t \sum_{h=0}^{N-1} \mathcal{E}_2^h + 2\Delta t \sum_{h=0}^{N-1} ||F_h||^2_{L^2(\Omega_2)}. \tag{35}$$

If $\Delta t < 2$, the left-hand side of the last inequality is positive, which allows us to bound each of its terms by the right-hand side. Exploiting this property, it is natural to consider the following inequality

$$\mathcal{E}_2^N \leq \frac{\Delta t}{1 - \frac{\Delta t}{2}} \sum_{h=0}^{N-1} \mathcal{E}_2^h + \frac{2\Delta t}{(1 - \frac{\Delta t}{2})} \sum_{h=0}^{N-1} ||F_h||^2_{L^2(\Omega_2)}.$$

By applying the discrete Gronwall lemma (see, *e.g.*, [34]), we observe that the energy in the subdomain Ω_2 is bounded from above by the problem data, indeed

$$\mathcal{E}_2^N \leq \frac{2\Delta t}{(1 - \frac{\Delta t}{2})} \sum_{h=0}^{N-1} ||F_h||^2_{L^2(\Omega_2)} \exp\left(\frac{T}{1 - \frac{\Delta t}{2}}\right). \tag{36}$$

From (35), it is also possible to derive a first estimate for $\mathcal{E}_1^N$, that is

$$\mathcal{E}_1^N \leq \Delta t \sum_{h=0}^{N-1} \mathcal{E}_2^h + 2\Delta t \sum_{h=0}^{N-1} ||F_h||^2_{L^2(\Omega_2)}. \tag{37}$$

The stability of the numerical scheme then follows immediately by using (36), which can be generalized to a generic instant $t_h < t_N = T$, to bound each term in the first summation on the right-hand side of the latter inequality, as done at the continuous level.

5 Numerical results

For simplicity of implementation, and for an initial investigation, we will limit our analysis to the case of matching meshes, geometrically conforming to the (polygonal approximation of the) boundary of the domains: $\mathcal{T}^{(2)}_{\widehat{\Delta x}} = \mathcal{T}^{(1)}_{\widetilde{\Delta x}}$, which implies $M = M_1$ and $\widehat{\Delta x} = \widetilde{\Delta x}$. The possibility of introducing non-matching meshes on the interface between the two domains Ω_1 and Ω_2 will be object of future work. Let us note that here we will deal with problems that have already been solved using the energetic BEM-FEM coupling in [3]; therefore, we will be able to compare the results obtained by the proposed Nitsche's BEM-FEM coupling with reference solutions. The model problem described in subsection 2.1 is specified as follows. Let $\Omega \subset \mathbb{R}^2$ be a circle with unit radius and let Γ_N be its boundary; $\mathbb{R}^2 \setminus \Omega$ is partitioned into two subdomains whose interface Γ is a circumference of radius 2, as visible in Figure 2. For all the simulations we fix $T = 20$.

Chosen Ω_2 as the FEM domain, we construct a mesh $\mathcal{T}^{(2)}_{\Delta x}$ for this subdomain, composed of 84 triangles, such that the boundary Γ_N and the interface Γ are approximated by 12 and 24 segments, respectively, each of length $\widetilde{\Delta x} \simeq 0.52$ (Figure 3). We associate this mesh with a time discretization parameter $\Delta t = 0.5$; then we work with two refinements obtained by halving both parameters, $\widetilde{\Delta x}$ and Δt (for the space meshes, see Figures 4 and 5).

5.1 Monodomain

Let us first assume that $\mathbb{R} \setminus \Omega$ is homogeneous, meaning that the wave speed is constant at each point, *i.e.*, $c_1 = c_2 = c$. In this case, the domain decomposition $\Omega^c = \Omega_1 \cup \Omega_2$ (Figure 2) is purely fictitious. To begin, we choose $c = 1$, obtained fixing unitary bulk modulus and unitary material density.

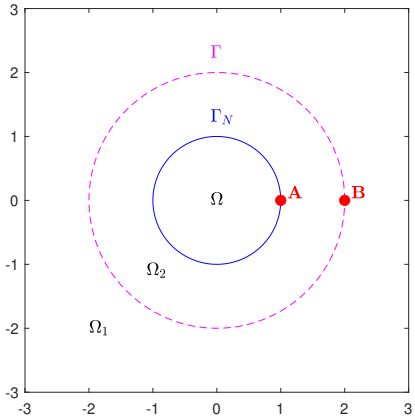

Figure 2: Problem domain.

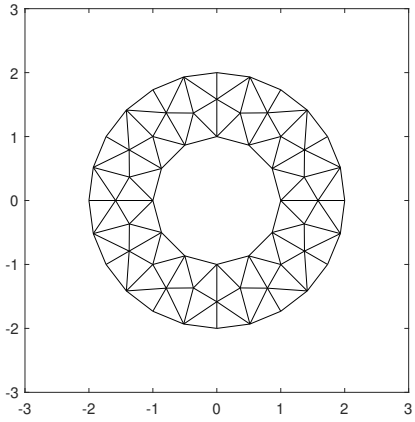

Figure 3: First triangulation of Ω_2 (on the boundaries $\widetilde{\Delta x} \simeq 0.52$).

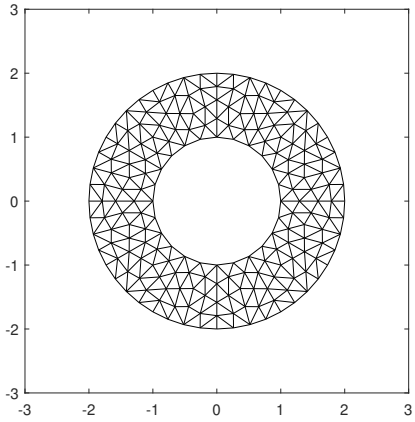

Figure 4: First mesh refinement of Ω_2 (on the boundaries $\widetilde{\Delta x} \simeq 0.26$).

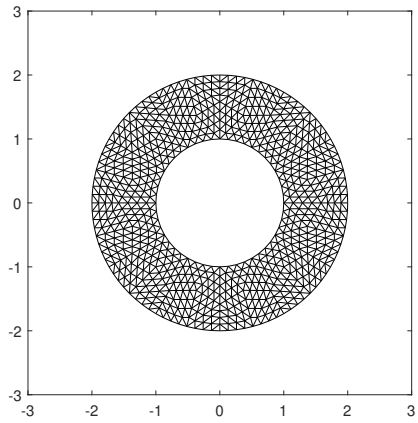

Figure 5: Second mesh refinement of Ω_2 (on the boundaries $\widetilde{\Delta x} \simeq 0.13$).

$\widetilde{\Delta x}$	Δt	$u_2^*(\mathbf{A}, 1)$	$u_2^*(\mathbf{A}, 5)$	$u_2^*(\mathbf{A}, 10)$	$u_2^*(\mathbf{A}, 15)$	$u_2^*(\mathbf{A}, 20)$
0.52	0.500	4.881012e-01	2.741009e-01	1.171168e-01	7.262682e-02	5.288077e-02
0.26	0.250	4.921792e-01	2.725877e-01	1.176549e-01	7.331935e-02	5.338217e-02
0.13	0.125	4.888554e-01	2.709984e-01	1.177424e-01	7.350866e-02	5.352144e-02

Table 1: Solution $u_2^*(\mathbf{A}, t)$ with $c = 1$, $\overline{\sigma}(\mathrm{x}, t) = e^{-t}$, $\theta = 0$ and $\chi = 1000$.

5.1.1 Exponential Neumann datum

Given the Neumann datum $\overline{\sigma}(x, t) = e^{-t}$, we are unable to solve the model problem analytically. Therefore, we are concerned with observing how the numerical solution varies at points **A** and **B** when we subject the initial mesh to two refinements. Values in Table 1 and Table 2 show that, as time increases, the solution in Ω_2 tends to stabilize under mesh refinements.

Unlike the BEM-FEM method, in the Nitsche's BEM-FEM coupling the continuity condition $u_1 = u_2$ on the interface is only weakly imposed. Therefore, we obtain two different approximate values of $u(\mathrm{x}, t)$ for each point on the interface: one considering the point belonging to the BEM-domain Ω_1, $u_1^*(\mathrm{x}, t)$, the other considering the point belonging to the FEM-domain Ω_2, $u_2^*(\mathrm{x}, t)$. The following Table 3 shows that these values are in optimal agreement in the point **B** of the interface Γ at different time instants.

Let us observe the behavior of the solution in Figure 6. This graph describes an explosive phenomenon, where the solution is maximum at the initial time instants and then decreases, until it almost runs out. Moreover, the solution in the point **B** is activated at $t = 1$, which is consistent with what is expected, since the interface Γ is located at a unit distance from the Neumann boundary Γ_N. As time increases, the curves $u_2^*(\mathbf{A}, t)$ and $u_2^*(\mathbf{B}, t)$ tend to overlap. As observed above, we note that the curves $u_2^*(\mathbf{B}, t)$ and $u_1^*(\mathbf{B}, t)$ seem to coincide.

$\widetilde{\Delta x}$	Δt	$u_2^*(\mathbf{B}, 1)$	$u_2^*(\mathbf{B}, 5)$	$u_2^*(\mathbf{B}, 10)$	$u_2^*(\mathbf{B}, 15)$	$u_2^*(\mathbf{B}, 20)$
0.52	0.500	8.945296e-02	2.737459e-01	1.188229e-01	7.301219e-02	5.302286e-02
0.26	0.250	7.548551e-02	2.732707e-01	1.191133e-01	7.367703e-02	5.351769e-02
0.13	0.125	5.925346e-02	2.723738e-01	1.191121e-01	7.385480e-02	5.365322e-02

Table 2: Solution $u_2^*(\mathbf{B}, t)$ with $c = 1$, $\overline{\sigma}(\mathrm{x}, t) = e^{-t}$, $\theta = 0$ and $\chi = 1000$.

$\widetilde{\Delta x}$	Δt	$u_1^*(\mathbf{B},1)$	$u_1^*(\mathbf{B},5)$	$u_1^*(\mathbf{B},10)$	$u_1^*(\mathbf{B},15)$	$u_1^*(\mathbf{B},20)$
0.52	0.500	8.949911e-02	2.738006e-01	1.188803e-01	7.307043e-02	5.308133e-02
0.26	0.250	7.550697e-02	2.732951e-01	1.191390e-01	7.370317e-02	5.354397e-02
0.13	0.125	5.926460e-02	2.723860e-01	1.191250e-01	7.386784e-02	5.366633e-02

Table 3: Solution $u_1^*(\mathbf{B},t)$ with $c=1$, $\overline{\sigma}(\mathrm{x},t)=e^{-t}$, $\theta=0$ and $\chi=1000$.

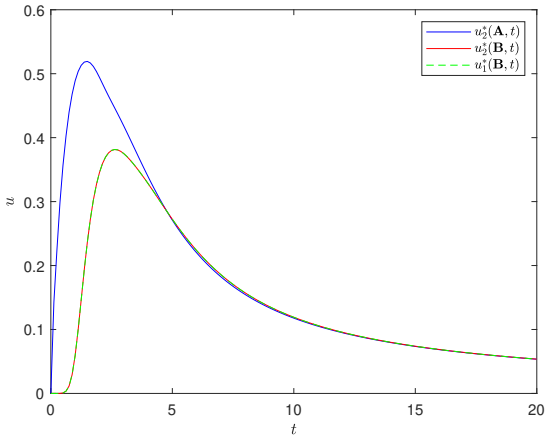

Figure 6: Graph of $u_2^*(\mathrm{x},\mathrm{t})$ in $\mathbf{A}$, $\mathbf{B}$ and $u_1^*(\mathrm{x},\mathrm{t})$ in $\mathbf{B}$ ($c=1$, $\overline{\sigma}(\mathrm{x},\mathrm{t})=\mathrm{e}^{-\mathrm{t}}$, $\theta=0$, $\chi=1000$).

On the interface Γ_I, since the values of $u_1^*(\mathrm{x},t)$ and $u_2^*(\mathrm{x},t)$ tend to coincide, we might also expect the same for the values of the respective fluxes in modulus. Table 4 shows a comparison between fluxes at two fixed time steps, the first and the last instants of the initial mesh. The BEM flux value $\sigma_1^*(\mathrm{x},t)$ is directly calculated by the algorithm, while a post-processing operation is required to obtain the FEM flux value $\sigma_2(u_2^*(\mathrm{x},t))$. The initial mesh is symmetric and uniformly distributed, so the FEM flux values across the different sides of the interface are equal to each other, and the same happens for BEM flux values. We report these values in the first row of Table 4. The same has been done for the refined meshes.

We can notice that BEM and FEM fluxes have opposite signs, consistent with what we expect. We observe that the two values are getting closer with slow convergence, which is most evident at the final time step. However, we would need much finer meshes to appreciate convergence.

On the boundary Γ_N, instead, we have imposed the Neumann condition $\sigma_2(u_2(\mathrm{x},t))=\overline{\sigma}(\mathrm{x},t)$. We therefore expect that the FEM flux calculated in post-processing will have the same sign and converge to the Neumann datum. Also in this case, Table 5 shows a hint of convergence. The sign difference between the two values at the final time step can be interpreted as a rough approximation of values tending towards zero.

$\widetilde{\Delta x}$	Δt	$t=0.5$		$t=20$	
		PP-FEM flux	BEM flux	PP-FEM flux	BEM flux
0.52	0.500	-9.266665e-02	2.468706e-02	2.142556e-04	-6.678668e-04
0.26	0.250	-5.251422e-02	1.782304e-02	2.327977e-04	-3.208727e-04
0.13	0.125	-1.326752e-02	5.351500e-03	2.386589e-04	-2.601043e-04

Table 4: Comparison between $\sigma_2(u_2^*(\mathrm{x},t))$ (PP-FEM flux) and $\sigma_1^*(\mathrm{x},t)$ (BEM flux) at two fixed time steps, for $\mathrm{x}\in\Gamma$ ($c=1$, $\overline{\sigma}(\mathrm{x},t)=e^{-t}$, $\theta=0$, $\chi=1000$).

$\widetilde{\Delta x}$	Δt	$t = 0.5$		$t = 20$	
		PP-FEM flux	Neumann datum	PP-FEM flux	Neumann datum
0.52	0.500	7.050191e-01	6.065307e-01	-6.821195e-05	2.061154e-09
0.26	0.250	5.505080e-01	6.065307e-01	-3.391231e-05	2.061154e-09
0.13	0.125	6.000707e-01	6.065307e-01	-1.719400e-05	2.061154e-09

Table 5: Comparison between $\sigma_2(u_2^*(\mathrm{x},t))$ (PP-FEM flux) and $\overline{\sigma}(\mathrm{x},t)$ (Neumann datum) at two fixed time steps, for $\mathrm{x} \in \Gamma_N$ ($c = 1$, $\overline{\sigma}(\mathrm{x},t) = e^{-t}$, $\theta = 0$, $\chi = 1000$).

$\widetilde{\Delta x}$	Δt	$u_2^*(\mathbf{A},1)$	$u_2^*(\mathbf{A},5)$	$u_2^*(\mathbf{A},10)$	$u_2^*(\mathbf{A},15)$	$u_2^*(\mathbf{A},20)$
0.52	0.500	8.293694e-01	2.214826e+00	2.944283e+00	3.355365e+00	3.643754e+00
0.26	0.250	8.205867e-01	2.234557e+00	2.963740e+00	3.379136e+00	3.670554e+00
0.13	0.125	8.113523e-01	2.241203e+00	2.969111e+00	3.385663e+00	3.677914e+00

Table 6: Solution $u_2^*(\mathbf{A},t)$ with $c = 1$, $\overline{\sigma}(\mathrm{x},t) = H(t)$, $\theta = 0$ and $\chi = 1000$.

5.1.2 Heaviside Neumann datum

Let us now consider the Neumann datum $\overline{\sigma}(\mathrm{x},t) = H(t)$. Repeating all the previous tests, related results are collected in Tables 6, 7, 8, 9, 10. The plot of the approximate solutions is reported in Figure 7. Similar considerations as before can be done.

5.1.3 Analyisis of the parameter χ

As it is known in case of time-independent problems [10] and as it has been proved in Section 4, the Nitsche's BEM-FEM coupling is stable when the Nitsche's parameter χ is large enough. Since we expect that, on the interface Γ, the approximate solutions $u_2^*(\mathbf{x},t)$, $u_1^*(\mathbf{x},t)$ tend to coincide for diminishing discretization parameters, in the following Tables we observe how the discrepancy $||u_2^*(\mathbf{B},t) - u_1^*(\mathbf{B},t)||_\infty$ varies for different values of the parameter χ. Looking at Tables 11, 12, related to the Neumann datum $\overline{\sigma}(x,t) = e^{-t}$, we can observe that, for small values of χ, the accuracy is very poor and the discrepancy does not improve at all refining the space and time meshes, while larger values χ allow to obtain a linear decay of the discrepancy w.r.t. the halving of $\widetilde{\Delta x}$ and Δt. Moreover, the larger the value of χ, the smaller the discrepancy of the two approximate solutions over the boundary on the whole time interval of analysis, *i.e.*, the closer the weak and strong imposition of continuity constraints between the BEM and FEM approximate solutions on $\Gamma \times [0,T]$. The same feature is visible in Tables 13, 14, related to the Neumann datum $\overline{\sigma}(x,t) = H(t)$.
In Figures 8 and 9, we report the errors $||u_2^*(\mathbf{B},t) - u_2^{ref}(\mathbf{B},t)||_\infty$ with respect to the reference solution obtained applying standard energetic BEM-FEM coupling on the finest space-time mesh, plotted w.r.t. the parameter χ, for both the considered Neumann data, respectively. If the Nitsche's parameter is too small, the errors are huge, then for growing χ they start diminishing until they stabilize (for $\chi \geq 10^1$ in relation to the exponential datum and for $\chi \geq 10^2$ for the Heaviside datum), at values depending linearly on the discretization parameters. This situation is clearly visible also looking at the graph of the approximate solutions in Figure 10 and in Figure 11: sensible graphs appear for $\chi = 10^1, 10^2$, respectively.

$\widetilde{\Delta x}$	Δt	$u_2^*(\mathbf{B},1)$	$u_2^*(\mathbf{B},5)$	$u_2^*(\mathbf{B},10)$	$u_2^*(\mathbf{B},15)$	$u_2^*(\mathbf{B},20)$
0.52	0.500	1.205855e-01	1.510063e+00	2.255060e+00	2.669033e+00	2.958353e+00
0.26	0.250	8.816702e-02	1.525252e+00	2.268471e+00	2.686477e+00	2.978761e+00
0.13	0.125	6.680492e-02	1.531368e+00	2.272363e+00	2.691449e+00	2.984553e+00

Table 7: Solution $u_2^*(\mathbf{B},t)$ with $c = 1$, $\overline{\sigma}(\mathrm{x},t) = H(t)$, $\theta = 0$ and $\chi = 1000$.

$\widetilde{\Delta x}$	Δt	$u_1^*(\mathbf{B},1)$	$u_1^*(\mathbf{B},5)$	$u_1^*(\mathbf{B},10)$	$u_1^*(\mathbf{B},15)$	$u_1^*(\mathbf{B},20)$
0.52	0.500	1.206486e-01	1.510375e+00	2.255655e+00	2.669918e+00	2.959531e+00
0.26	0.250	8.821112e-02	1.525437e+00	2.268817e+00	2.686989e+00	2.979441e+00
0.13	0.125	6.682763e-02	1.531463e+00	2.272541e+00	2.691712e+00	2.984903e+00

Table 8: Solution $u_1^*(\mathbf{B},t)$ with $c=1$, $\overline{\sigma}(\mathrm{x},t)=H(t)$, $\theta=0$ and $\chi=1000$.

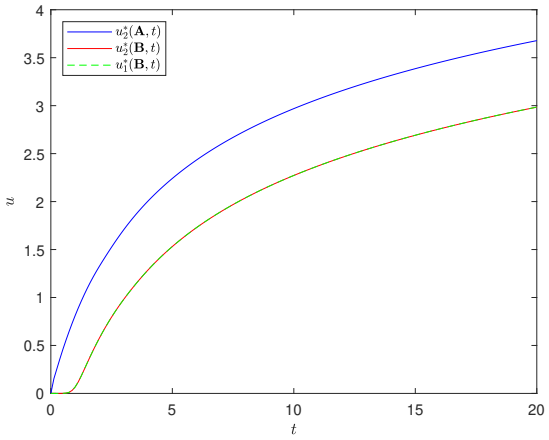

Figure 7: Graph of $u_2^*(\mathrm{x},\mathrm{t})$ in $\mathbf{A}$, $\mathbf{B}$ and $u_1^*(\mathrm{x},\mathrm{t})$ in $\mathbf{B}$ ($c=1$, $\overline{\sigma}(\mathrm{x},\mathrm{t})=\mathrm{H(t)}$, $\theta=0$, $\chi=1000$).

$\widetilde{\Delta x}$	Δt	$t=0.5$		$t=20$	
		PP-FEM flux	BEM flux	PP-FEM flux	BEM flux
0.52	0.500	-1.177559e-01	3.137101e-02	-5.580118e-01	4.965300e-01
0.26	0.250	-5.853290e-02	1.864238e-02	-5.352607e-01	5.014165e-01
0.13	0.125	-1.397994e-02	5.745389e-03	-5.192417e-01	5.024328e-01

Table 9: Comparison between $\sigma_2(u_2^*(\mathrm{x},t))$ (PP-FEM flux) and $\sigma_1^*(\mathrm{x},t)$ (BEM flux) at two fixed time steps, for $\mathrm{x}\in\Gamma$ ($c=1$, $\overline{\sigma}(\mathrm{x},t)=H(t)$, $\theta=0$, $\chi=1000$).

$\widetilde{\Delta x}$	Δt	$t=0.5$		$t=20$	
		PP-FEM flux	Neumann datum	PP-FEM flux	Neumann datum
0.52	0.500	8.959009e-01	1	7.658137e-01	1
0.26	0.250	8.751325e-01	1	8.507825e-01	1
0.13	0.125	9.506136e-01	1	9.257623e-01	1

Table 10: Comparison between $\sigma_2(u_2^*(\mathrm{x},t))$ (PP-FEM flux) and $\overline{\sigma}(\mathrm{x},t)$ (Neumann datum) at two fixed time steps, for $\mathrm{x}\in\Gamma_N$ ($c=1$, $\overline{\sigma}(\mathrm{x},t)=H(t)$, $\theta=0$, $\chi=1000$).

$\widetilde{\Delta x}$	Δt	χ				
		10^{-1}	10^{-2}	10^{-3}	10^{-4}	10^{-5}
0.52	0.500	6.021632e-01	5.019376e+00	1.048066e+01	1.148164e+01	1.158921e+01
0.26	0.250	3.928059e-01	2.889833e+00	9.074562e+00	1.071530e+01	1.090209e+01
0.13	0.125	2.290552e-01	1.603362e+00	7.458530e+00	1.006522e+01	1.039494e+01

Table 11: Discrepancy $||u_2^*(\mathbf{B},t) - u_1^*(\mathbf{B},t)||_\infty$ as χ varies ($c = 1$, $\overline{\sigma}(\mathrm{x},t) = e^{-t}$, $\theta = 0$).

$\widetilde{\Delta x}$	Δt	χ				
		10^{0}	10^{1}	10^{2}	10^{3}	10^{4}
0.52	0.500	7.699931e-02	7.495257e-03	7.399540e-04	7.388155e-05	7.386997e-06
0.26	0.250	4.261052e-02	3.655366e-03	3.515315e-04	3.499517e-05	3.497917e-06
0.13	0.125	2.270310e-02	1.972287e-03	1.864151e-04	1.852532e-05	1.851344e-06

Table 12: Discrepancy $||u_2^*(\mathbf{B},t) - u_1^*(\mathbf{B},t)||_\infty$ as χ varies ($c = 1$, $\overline{\sigma}(\mathrm{x},t) = e^{-t}$, $\theta = 0$).

Finally, since in Section 4 we give the expression $\chi = \frac{\chi_0}{\Delta x}$, in Tables 15 and 16 we show the discrepancies between the BEM and FEM approximate solutions over the interface for three different values of the parameter χ_0. In this respect, we can appreciate a quadratic decay of the discrepancies w.r.t. the discretization parameters, since for a fixed χ_0, χ doubles as they halve.

5.2 Bidomain

From now on, we will consider only the Neumann datum $\overline{\sigma}(\mathrm{x},t) = H(t)$. All the graphs in this subsection were obtained using the second mesh ($\widetilde{\Delta x} \simeq 0.26$ and $\Delta t = 0.25$). Before considering the case $c_1 \neq c_2$, let us observe what happens to a monodomain when we vary the wave speed. In Figure 12, we set $c_1 = c_2 = c = 2$, considering unitary bulk moduli and material densities $\rho_1 = \rho_2 = 0.25$. This Figure has to be compared to Figure 7. Obviously, the solution to the problem depends on c: if we double it, the curves corresponding to $u_2^*(\mathbf{A},t)$ and $u_2^*(\mathbf{B},t)$ reach larger values at the end of the time interval of analysis $T = 20$, the perturbation takes half the time to reach $\mathbf{B}$ and in general takes half time to reach the same values of the curves in Figure 7.

When the domain Ω^c is not homogeneous, the interface Γ is no longer fictitious, since it separates two regions with different speeds. In particular, on the geometry studied in the previous subsection, we assume that the speeds in Ω_1 and Ω_2 are twice each other, focusing on the case $c_1 = 1$ and $c_2 = 2$ as well as on the case $c_1 = 2$ and $c_2 = 1$.

From the graphs in Figure 13, we note that as long as the perturbation is localized in Ω_2, $u_2^*(\mathbf{A},t)$ behaves as in the case of a monodomain with the same physical characteristics as Ω_2. When the wave crosses the interface Γ, diffraction and reflection phenomena occur, as a result of which the value of the solution can no longer be clearly associated with one of the two monodomains. As time progresses, $u_2^*(\mathbf{A},t)$ tends to follow the behavior it would have in a monodomain with the same physical characteristics as Ω_1. The obtained results are in perfect agreement with those reported in [3].

To complete the analysis, we present in Figure 14 the behavior of the approximate solutions in a bidomain with the same geometrical configuration and the same two speeds as before, but where the larger speed is obtained fixing unitary density and quadruplicating the corresponding bulk modulus. Let us note that in this case the normal derivative of the solution along the Neumann boundary is divided by four when the speed of the FEM subdomain is doubled and therefore the perturbation is weaker. In both cases shown in Figure 14, at the beginning of the simulation the approximate solutions in the point $\mathbf{A}$ lie on the curve representing the solution in a monodomain constituted by the same material of Ω_2, but after the wave solicited by the

$\widetilde{\Delta x}$	Δt	χ				
		10^{-1}	10^{-2}	10^{-3}	10^{-4}	10^{-5}
0.52	0.500	1.151597e+01	6.950545e+01	1.189715e+02	1.270768e+02	1.279358e+02
0.26	0.250	6.094376e+00	4.734729e+01	1.146800e+02	1.302859e+02	1.320313e+02
0.13	0.125	2.993582e+00	2.652913e+01	9.817770e+01	1.252313e+02	1.285870e+02

Table 13: Discrepancy $||u_2^*(\mathbf{B},t) - u_1^*(\mathbf{B},t)||_\infty$ as χ varies ($c = 1$, $\overline{\sigma}(\mathrm{x},t) = H(t)$, $\theta = 0$).

$\widetilde{\Delta x}$	Δt	χ				
		10^0	10^1	10^2	10^3	10^4
0.52	0.500	1.205896e+00	1.205586e-01	1.185195e-02	1.177544e-03	1.176621e-04
0.26	0.250	6.240120e-01	6.311591e-02	6.615496e-03	6.799844e-04	6.825243e-05
0.13	0.125	3.033172e-01	3.092636e-02	3.341269e-03	3.497720e-04	3.519633e-05

Table 14: Discrepancy $||u_2^*(\mathbf{B},t) - u_1^*(\mathbf{B},t)||_\infty$ as χ varies ($c = 1$, $\overline{\sigma}(\mathrm{x},t) = H(t)$, $\theta = 0$).

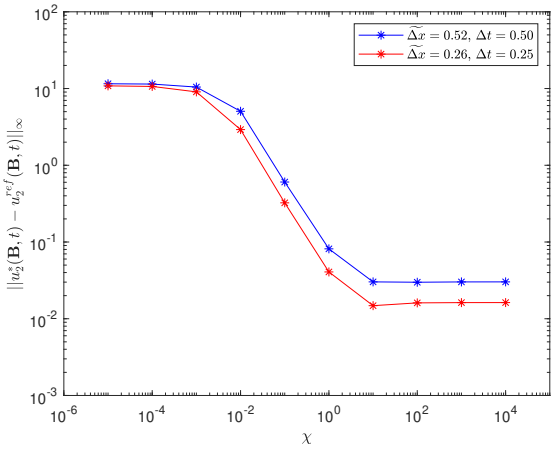

Figure 8: Error $||u_2^*(\mathbf{B},t) - u_2^{ref}(\mathbf{B},t)||_\infty$ as χ varies ($c = 1$, $\overline{\sigma}(\mathrm{x},t) = e^{-t}$, $\theta = 0$).

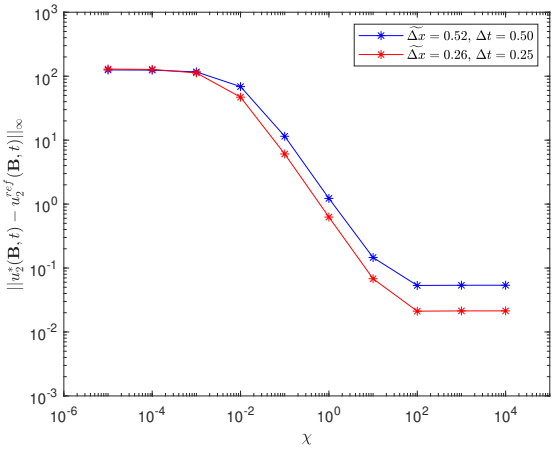

Figure 9: Error $||u_2^*(\mathbf{B},t) - u_2^{ref}(\mathbf{B},t)||_\infty$ as χ varies ($c = 1$, $\overline{\sigma}(\mathrm{x},t) = H(t)$, $\theta = 0$).

$\widetilde{\Delta x}$	Δt	χ_0		
		1	10	100
0.52	0.500	4.298161e-02	4.173342e-03	4.140684e-04
0.26	0.250	1.084176e-02	9.928493e-04	9.807653e-05
0.13	0.125	2.812750e-03	2.616817e-04	2.594266e-05

Table 15: Discrepancy $||u_2^*(\mathbf{B},t) - u_1^*(\mathbf{B},t)||_\infty$ as γ_0 varies, $\chi = \chi_0/\Delta x$ ($c = 1$, $\overline{\sigma}(\mathrm{x},t) = e^{-t}$, $\theta = 0$).

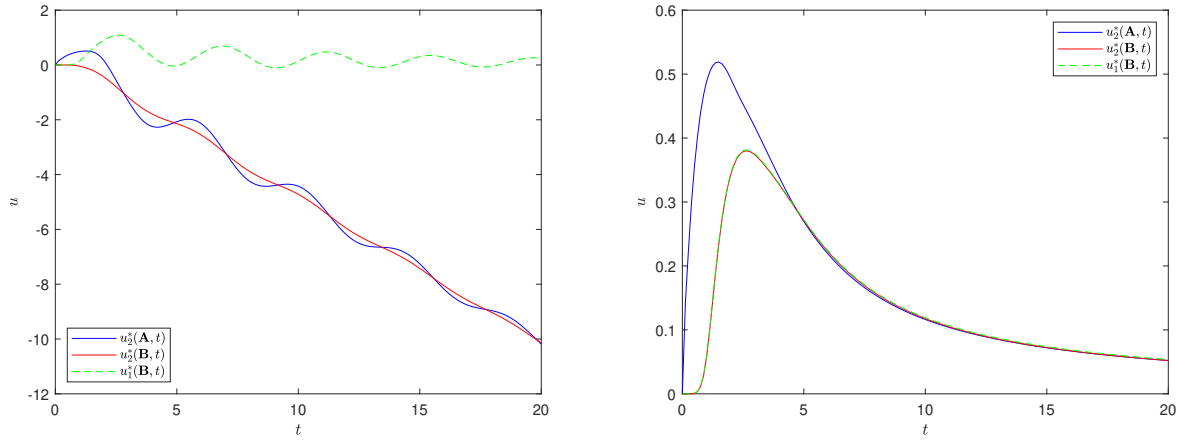

Figure 10: Graph of $u_2^*(\mathrm{x},\mathrm{t})$ in $\mathbf{A}$, $\mathbf{B}$ and $u_1^*(\mathrm{x},\mathrm{t})$ in $\mathbf{B}$, for $\chi = 10^{-5}$ (left), $\chi = 10^{1}$ (right) ($c = 1$, $\overline{\sigma}(\mathrm{x},\mathrm{t}) = \mathrm{e}^{-\mathrm{t}}$, $\theta = 0$).

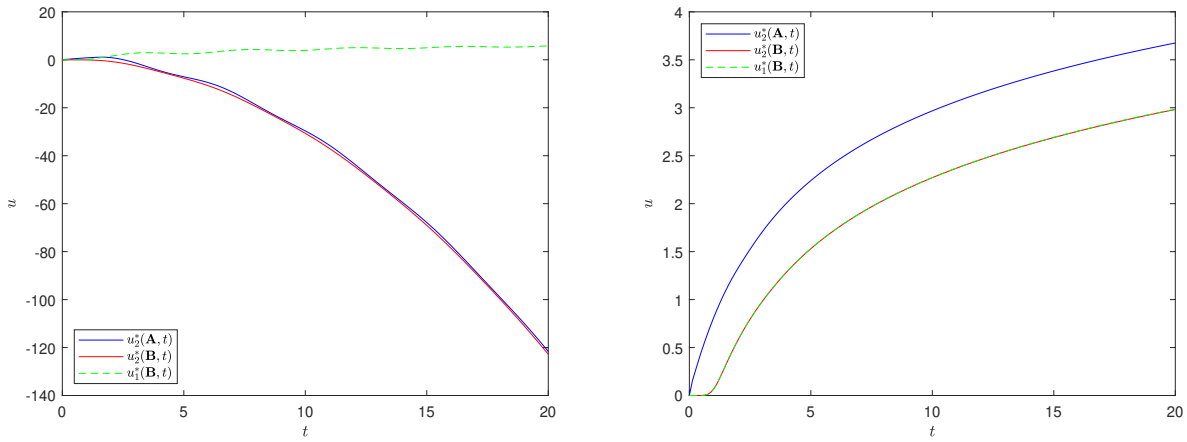

Figure 11: Graph of $u_2^*(\mathrm{x},\mathrm{t})$ in $\mathbf{A}$, $\mathbf{B}$ and $u_1^*(\mathrm{x},\mathrm{t})$ in $\mathbf{B}$, for $\chi = 10^{-5}$ (left), $\chi = 10^{2}$ (right) ($c = 1$, $\overline{\sigma}(\mathrm{x},\mathrm{t}) = \mathrm{H}(\mathrm{t})$, $\theta = 0$).

$\widetilde{\Delta x}$	Δt	χ_0		
		1	10	100
0.52	0.500	6.765145e-01	6.728230e-02	6.618045e-03
0.26	0.250	1.755019e-01	1.805583e-02	1.891014e-03
0.13	0.125	4.307223e-02	4.615621e-03	4.883787e-04

Table 16: Discrepancy $||u_2^*(\mathbf{B},t) - u_1^*(\mathbf{B},t)||_\infty$ as χ_0 varies, $\chi = \chi_0/\Delta x$ ($c = 1$, $\overline{\sigma}(\mathrm{x},t) = H(t)$, $\theta = 0$).

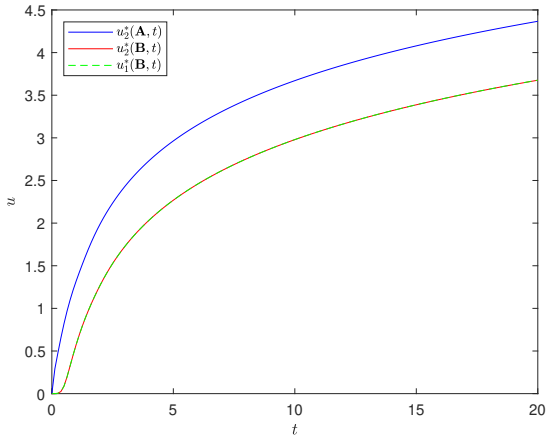

Figure 12: Graph of $u_2^*(\mathrm{x},t)$ in $\mathbf{A}$, $\mathbf{B}$ and $u_1^*(\mathrm{x},t)$ in $\mathbf{B}$ ($c=2$, $\overline{\sigma}(\mathrm{x},t)=H(t)$, $\theta=0$, $\chi=1000$).

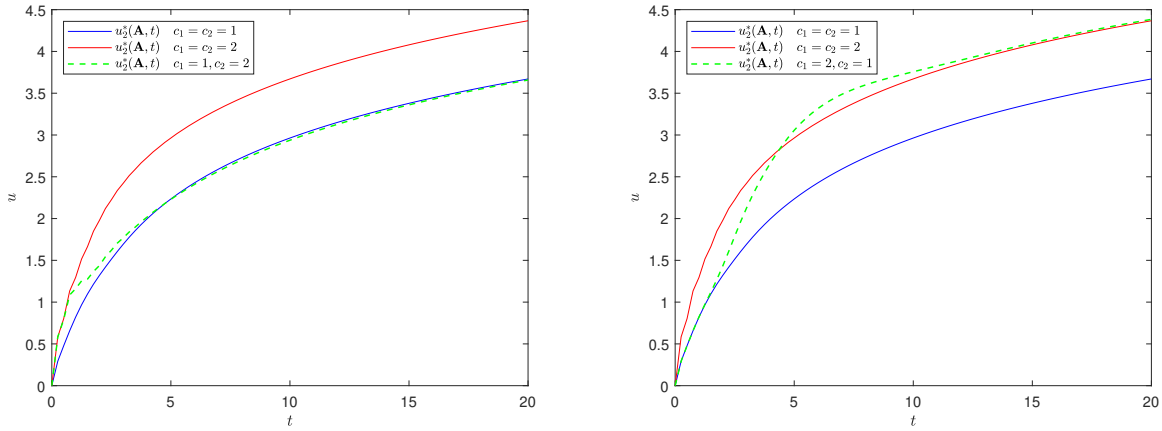

Figure 13: Graph of $u_2^*(\mathbf{A},t)$ in the bidomain with different material densities and unitary bulk moduli ($\overline{\sigma}(\mathrm{x},t)=H(t)$, $\theta=0$, $\chi=1000$).

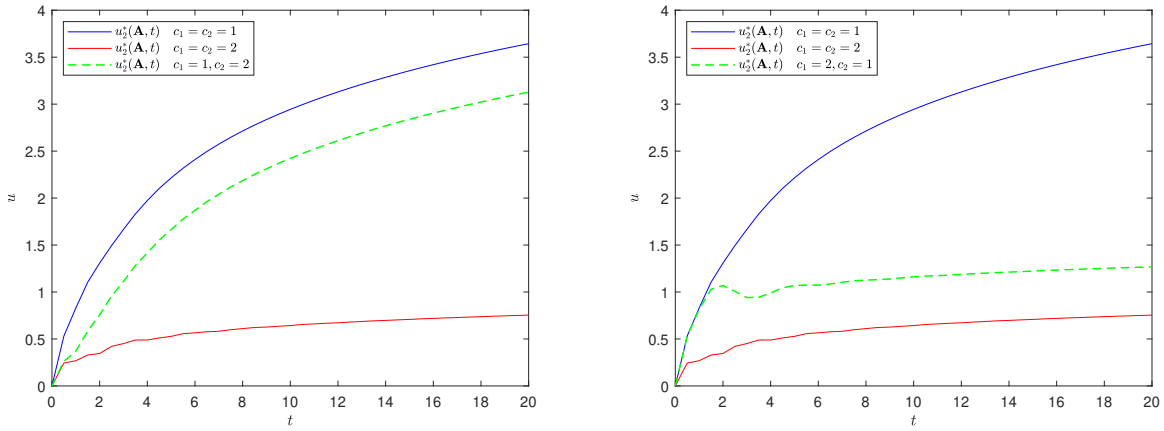

Figure 14: Graph of $u_2^*(\mathbf{A},t)$ in the bidomain with different bulk moduli and unitary material densities ($\overline{\sigma}(\mathrm{x},t)=H(t)$, $\theta=0$, $\chi=1000$).

boundary datum has reached the interface and the reflected wave has come back to the Neumann boundary ($t=1$ when $c_2=2$, $t=2$ when $c_2=1$), the approximate solutions assume the behavior of the solution related to a monodomain constituted by the same material of the unbounded subdomain Ω_1, even if not overlapping it as before. Finally, let us observe that, even if all the bidomain plots are presented for $\chi=10^3$, analogous results have been obtained for $\chi\geq 10^2$.

Acknowledgements

Franz Chouly thanks the Italian National Institute for Advanced Mathematics (INdAM, Istituto Nazionale di Alta Matematica) for funding and the University of Parma for hosting during his visiting position. The authors thank Giulia di Credico and Heiko Gimperlein for stimulating discussions.

References

[1] T. Abboud, P. Joly, J. Rodríguez, and I. Terrasse, *Coupling discontinuous Galerkin methods and retarded potentials for transient wave propagation on unbounded domains*, Journal of Computational Physics, 230 (2011), pp. 5877–5907.

[2] R.-A. Adams, *Sobolev spaces*, vol. 65 of Pure and Applied Mathematics, Academic Press, New York-London, 1975.

[3] A. Aimi, L. Desiderio, M. Diligenti, and C. Guardasoni, *A numerical study of energetic BEM-FEM applied to wave propagation in 2D multidomains*, Publications de l'Institut Mathématique. Nouvelle Série, 96 (2014), pp. 5–22.

[4] A. Aimi, G. Di Credico, and H. Gimperlein, *Space-time boundary elements for frictional contact in elastodynamics*, Computer Methods in Applied Mechanics and Engineering, 427 (2024), p. 25. Id/No 117066.

[5] A. Aimi, G. Di Credico, H. Gimperlein, C. Guardasoni, and G. Speroni, *Weak imposition of boundary conditions for the boundary element method in the time domain*, Applied Numerical Mathematics, 200 (2024), pp. 18–42.

[6] A. Aimi, M. Diligenti, A. Frangi, and C. Guardasoni, *Energetic BEM-FEM coupling for wave propagation in 3D multidomains*, International Journal for Numerical Methods in Engineering, 97 (2014), pp. 377–394.

[7] L. Banjai, *Implicit/explicit, BEM/FEM coupled scheme for acoustic waves with the wave equation in the second order formulation*, Computational Methods in Applied Mathematics, 22 (2022), pp. 757–773.

[8] L. Banjai, C. Lubich, and F.-J. Sayas, *Stable numerical coupling of exterior and interior problems for the wave equation*, Numerische Mathematik, 129 (2015), pp. 611–646.

[9] R. Becker, P. Hansbo, and R. Stenberg, *A finite element method for domain decomposition with non-matching grids.*, M2AN. Mathematical Modelling and Numerical Analysis. ESAIM, European Series in Applied and Industrial Mathematics, 37 (2003), pp. 209–225.

[10] T. Betcke, M. Bosy, and E. Burman, *Hybrid coupling of finite element and boundary element methods using Nitsche's method and the Calderón projection*, Numerical Algorithms, 91 (2022), pp. 997–1019.

[11] M. Bonnet, A. Burel, M. Duruflé, and P. Joly, *Effective transmission conditions for thin-layer transmission problems in elastodynamics. the case of a planar layer model*, European Series in Applied and Industrial Mathematics (ESAIM): Mathematical Modelling and Numerical Analysis, 50 (2016), pp. 43–75.

[12] F. Brezzi and C. Johnson, *On the coupling of boundary integral and finite element methods*, Calcolo, 16 (1979), pp. 189–201.

[13] F. Brezzi, C. Johnson, and J. C. Nedelec, *On the coupling of boundary integral and finite element methods*. Basic problems of numerical mathematics, 4th Symp., Plezn/CSSR 1978, 103–114 (1978), 1978.

[14] A. Burel, S. Impériale, and P. Joly, *Solving the homogeneous isotropic linear elastodynamics equations using potentials and finite elements. The case of the rigid boundary condition*, Sibirskiĭ Zhurnal Vychislitel'noĭ Matematiki, 15 (2012), pp. 165–174.

[15] F. Chouly, *Finite element approximation of boundary value problems*, Compact Textbooks in Mathematics, Birkhäuser/Springer, Cham, 2025. With a foreword by Stéphane Bordas.

[16] ——, *A review on some discrete variational techniques for the approximation of essential boundary conditions*, Vietnam Journal of Mathematics, 54 (2026), pp. 73–115.

[17] M. Duval, J.-C. Passieux, M. Salaün, and S. Guinard, *Non-intrusive coupling: recent advances and scalable nonlinear domain decomposition*, Archives of Computational Methods in Engineering, 23 (2016), pp. 17–38.

[18] A. Ern and J.-L. Guermond, *Finite elements II—Galerkin approximation, elliptic and mixed PDEs*, vol. 73 of Texts in Applied Mathematics, Springer, Cham, 2021.

[19] ——, *Finite elements III—first-order and time-dependent PDEs*, vol. 74 of Texts in Applied Mathematics, Springer, Cham, 2021.

[20] S. Falletta, *BEM coupling with the FEM fictitious domain approach for the solution of the exterior Poisson problem and of wave scattering by rotating rigid bodies*, IMA Journal of Numerical Analysis, 38 (2018), pp. 779–809.

[21] A. Fritz, S. Hüeber, and B. I. Wohlmuth, *A comparison of mortar and Nitsche techniques for linear elasticity*, Calcolo, 41 (2004), pp. 115–137.

[22] T. Führer, G. Gantner, and M. Karkulik, *Space-time FEM-BEM couplings for parabolic transmission problems*, SIAM Journal on Numerical Analysis, 63 (2025), pp. 1909–1932.

[23] T. Gustafsson, P. Råback, and J. Videman, *Mortaring for linear elasticity using mixed and stabilized finite elements*, Computer Methods in Applied Mechanics and Engineering, 404 (2023), p. 13. Id/No 115796.

[24] P. Hansbo, *Nitsche's method for interface problems in computational mechanics*, GAMM-Mitteilungen, 28 (2005), pp. 183–206.

[25] Q. Hu, F. Chouly, P. Hu, G. Cheng, and S. P. A. Bordas, *Skew-symmetric Nitsche's formulation in isogeometric analysis: Dirichlet and symmetry conditions, patch coupling and frictionless contact*, Computer Methods in Applied Mechanics and Engineering, 341 (2018), pp. 188–220.

[26] C. Johnson and J. C. Nedelec, *On the coupling of boundary integral and finite element methods*, Mathematics of Computation, 35 (1980), pp. 1063–1079.

[27] E. Khattatov and I. Yotov, *Domain decomposition and multiscale mortar mixed finite element methods for linear elasticity with weak stress symmetry*, European Series in Applied and Industrial Mathematics (ESAIM): Mathematical Modelling and Numerical Analysis, 53 (2019), pp. 2081–2108.

[28] V. A. Kovtunenko, A. Petrov, and Y. Renard, *Space-time fem solution of dynamic contact problem with discontinuous velocity for multiple impact of deformed bar using pdas method*, Mathematical Methods in the Applied Sciences, (2025). Available online. `https://doi.org/10.1002/mma.70370`.

[29] J. A. Martínez, S. Imperiale, P. Joly, and J. Rodríguez, *Numerical analysis of a method for solving 2D linear isotropic elastodynamics with traction free boundary condition using potentials and finite elements*, Mathematics of Computation, 90 (2021), pp. 1589–1636.

[30] V. G. Maz'ja, *Sobolev spaces*, Springer Series in Soviet Mathematics, Springer-Verlag, Berlin, 1985. Translated from the Russian by T. O. Shaposhnikova.

[31] W. McLean, *Strongly elliptic systems and boundary integral equations*, Cambridge University Press, Cambridge, 2000.

[32] V. P. Nguyen, P. Kerfriden, M. Brino, S. P. A. Bordas, and E. Bonisoli, *Nitsche's method for two and three dimensional NURBS patch coupling*, Computational Mechanics, 53 (2014), pp. 1163–1182.

[33] J. Nitsche, *Über ein Variationsprinzip zur Lösung von Dirichlet-Problemen bei Verwendung von Teilräumen, die keinen Randbedingungen unterworfen sind*, Abhandlungen aus dem Mathematischen Seminar der Universität Hamburg, 36 (1971), pp. 9–15.

[34] A. Quarteroni and A. Valli, *Numerical approximation of partial differential equations*, Springer, 1994.

[35] J. D. Sanders, T. A. Laursen, and M. A. Puso, *A Nitsche embedded mesh method*, Computational Mechanics, 49 (2012), pp. 243–257.

[36] F.-J. Sayas, *The validity of Johnson-Nédélec's BEM-FEM coupling on polygonal interfaces*, SIAM Review, 55 (2013), pp. 131–146.

[37] O. Steinbach and C. Urzúa-Torres, *A new approach to space-time boundary integral equations for the wave equation*, SIAM Journal on Mathematical Analysis, 54 (2022), pp. 1370–1392.

[38] R. Stenberg, *On some techniques for approximating boundary conditions in the finite element method*, Journal of Computational and Applied Mathematics, 63 (1995), pp. 139–148.

[39] V. Thomée, *Galerkin finite element methods for parabolic problems*, vol. 25 of Springer Series in Computational Mathematics, Springer-Verlag, Berlin, 1997.

[40] O. C. Zienkiewicz, D. W. Kelly, and P. Bettess, *The coupling of the finite element method and boundary solution procedures*, International Journal for Numerical Methods in Engineering, 11 (1977), pp. 355–375.